Cold-water corals and hydrocarbon-rich seepage in the Pompeia Province (Gulf of Cádiz) — living on the edge

Blanca Rincón-Tomás[1], Jan-Peter Duda[2], Luis Somoza[3], Francisco Javier González[3], Dominik Schneider[1], Teresa Medialdea[3], Esther Santofimia[4], Enrique López-Pamo[4], Pedro Madureira[5], Michael Hoppert[1], and Joachim Reitner[6,7]

[1]Georg-August-University Göttingen, Institute of Microbiology and Genetics, Grisebachstraße 8, 37077 Göttingen, Germany
[2]Department of Earth Sciences, University of California Riverside, CA 92521, USA
[3]Marine Geology Dept., Geological Survey of Spain, IGME, Ríos Rosas 23, 28003 Madrid, Spain
[4]Geological Resources Dept., Geological Survey of Spain, IGME, Ríos Rosas 23, 28003 Madrid, Spain
[5]Estrutura de Missão para a Extensão da Plataforma Continental (EMEPC). Rua Costa Pinto 165, 2770-047 Paço de Arcos, Portugal
[6]Georg-August-University Göttingen, Göttingen Centre of Geosciences, Goldschmidtstraße 3, 37077 Göttingen, [7]Germany[3]Göttingen Academy of Sciences and Humanities, Theaterstraße 7, 37073 Göttingen, Germany

Correspondence to: Blanca Rincón-Tomás (b.rincontomas@gmail.com)

Abstract. Azooxanthellate cold-water corals (CWCs) have a global distribution and have commonly been found in areas of active fluid seepage. The relationship between the CWCs and these fluids, however, is not well understood. This study aims at unraveling the relationship between CWC development and hydrocarbon-rich seepage in the Pompeia Province (Gulf of Cádiz, Atlantic Ocean). This region comprises mud volcanoes, coral ridges and fields of coral mounds, which are all affected by the tectonically driven seepage of hydrocarbon-rich fluids. The type of seepage such as focused, scattered, diffused or eruptive, is tightly controlled by a complex system of faults and diapirs. Early diagenetic carbonates from the currently active Al Gacel MV exhibit δ^{13}C-signatures down to −28.77 ‰ VPDB, indicating biologically derived methane as the main carbon source. The same samples contain ^{13}C-depleted lipid biomarkers diagnostic for archaea such as crocetane (δ^{13}C down to −101.2 ‰ VPDB) and PMI (δ^{13}C down to −102.9 ‰ VPDB), evidencing microbially mediated anaerobic oxidation of methane (AOM). This is further supported by next generation DNA sequencing data, demonstrating the presence of AOM related microorganisms (ANME archaea, sulfate-reducing bacteria) in the carbonate. Embedded corals in some of the carbonates and CWC fragments exhibit less negative δ^{13}C values (−8.08 to −1.39‰ VPDB), pointing against the use of methane as the carbon source. Likewise, the absence of DNA from methane- and sulfide-oxidizing microbes in a sampled coral does not support a chemosynthetic lifestyle of these organisms. In the light of these findings, it appears that the CWCs benefit rather indirectly from hydrocarbon-rich seepage by using methane-derived authigenic carbonates as a substratum for colonization. At the same time, chemosynthetic organisms at active sites prevent coral dissolution and necrosis by feeding on the seeping fluids (i. e. methane, sulfate, hydrogen sulfide), allowing cold-water corals to colonize carbonates currently affected by hydrocarbon-rich seepage.

1. Introduction

Cold-water corals (CWCs) are a widespread, non-phylogenetic group of cnidarians that include hard skeleton scleractinian corals, soft-tissue octocorals, gold corals, black corals and hydrocorals (Roberts et al., 2006; Roberts et al., 2009; Cordes et al., 2016). Typically, they thrive at low temperatures (4 – 12 ºC) and occur in water depths

of ca. 50 – 4000 m. CWCs are azooxanthellate and solely rely on their nutrition as energy and carbon sources (Roberts et al., 2009). Some scleractinian corals (e.g. *Lophelia pertusa*, *Madrepora oculata*, *Dendrophyllia cornigera*, *Dendrophyllia alternata*, *Eguchipsammia cornucopia*) are able to form colonies or even large carbonate mounds (Rogers et al., 1999; Wienberg et al., 2009; Watling et al., 2011; Somoza et al., 2014). Large vertical mounds and elongated ridges formed by episodic growth of scleractinian corals (mainly *Lophelia pertusa*) are for instance widely distributed along the continental margins of the Atlantic Ocean (Roberts et al., 2009). These systems are of great ecological value since they offer sites for resting-, breeding-, and feeding for various invertebrates and fishes (Cordes et al., 2016 and references therein).

Several environmental forces influence the initial settling, growth, and decline of CWCs. These include, among others, an availability of suitable substrates for coral larvae settlement, low sedimentation rates, oceanographic boundary conditions (e.g. salinity, temperature and density of the ocean water) and a sufficient supply of nutrients through topographically controlled currents systems (Mortensen et al., 2001; Roberts et al., 2003; Thiem et al., 2006; Dorschel et al., 2007; Dullo et al., 2008; Van Rooij et al., 2011; Hebbeln et al., 2016). Alternatively, the "hydraulic theory" suggests that CWC ecosystems may be directly fueled by fluid seepage, providing a source of e.g. sulfur compounds, nitrogen compounds, P, CO_2 and/or hydrocarbons (Hovland, 1990; Hovland and Thomsen, 1997; Hovland et al., 1998; 2012). This relationship is supported by the common co-occurrence of CWC-mounds and hydrocarbon-rich seeps around the world, for example at the Hikurangi Margin in New Zealand (Liebetrau et al., 2010), the Brazil margin (e.g. Gomes-Sumida et al., 2004), the Darwin Mounds in the northern Rockall Trough (Huvenne et al., 2009), the Kristin field on the Norwegian shelf (Hovland et al., 2012), the western Alborán Sea (Margreth et al., 2011), and the Gulf of Cádiz (e.g. Díaz-del-Río et al., 2003; Foubert et al., 2008). However, CWCs may also benefit rather indirectly from seepage. For instance, methane-derived authigenic carbonates (MDACs) formed through the microbially mediated anaerobic oxidation of methane (AOM; Suess & Whiticar, 1989; Hinrichs et al., 1999; Thiel et al., 1999; Boetius et al., 2000; Hinrichs & Boetius, 2002) potentially provide hard substrata for larval settlement (e.g. Díaz-del-Rio et al., 2003; Van Rooij et al., 2011; Magalhães et al. 2012; Le Bris et al., 2016; Rueda et al., 2016). In addition, larger hydrocarbon-rich seepage related structures such as mud volcanoes and carbonate mud mounds act as morphological barriers favoring turbulent water currents that deliver nutrients to the corals (Roberts et al., 2009; Wienberg et al., 2009; Margreth et al., 2011; Vandorpe et al., 2016).

In the Gulf of Cádiz, most CWC occurrences are "coral graveyards" with only a few living corals that are situated along the Iberian and Moroccan margins. These CWC systems are typically associated with diapiric ridges, steep fault-controlled escarpments, and mud volcanoes (MVs) such as the Faro MV, Hesperides MV, Mekness MV, and mud volcanoes in the Pen Duick Mud Volcano Province (Foubert et al., 2008; Wienberg et al., 2009). Mud volcanoes (and other conspicuous morphological structures in this region such as pockmarks) are formed through tectonically induced fluid flow (Pinheiro et al., 2003; Somoza et al., 2003; Medialdea et al., 2009; León et al., 2010; 2012). The fluid flow is promoted through the of the high regional tectonic activity and high fluid contents of sediments in this area (mainly CH_4 and, to a lesser extent, H_2S, CO_2, and N_2: Pinheiro et al., 2003; Hensen et al., 2007; Scholz et al., 2009; Smith et al., 2010; González et al., 2012). However, the exact influence of fluid flow on CWC growth in this region remains elusive.

This study aims at elucidating the linkage between the present-day formation of MDACs and CWCs development, by testing whether CWCs are indeed non-chemosynthetic fauna or harbor in fact chemosynthetic symbionts which allow them consuming some of the reduced compounds in sites of active emission of under seafloor fluids. We

address our hypothesis by the combined analyses of high-resolution ROV underwater images, geophysical data (e.g. seabed topography, deep high-resolution multichannel seismic reflection data), and sample materials (water analysis, petrographic features, $\delta^{13}C$- and $\delta^{18}O$-signatures of carbonates, lipid biomarkers and environmental 16s rDNA sequences of the prokaryotic microbial community). We focus our study in the Pompeia Province (**Fig. 1**), which encompasses mud volcanoes as the currently active Al Gacel MV (León et al., 2012), diapiric coral ridges and mounds. Based on our findings, we propose an integrated model to explain the tempo-spatial and genetic relations between CWCs, chemosynthetic fauna and hydrocarbon-rich seepage in the study area.

2. Materials and Methods

This study is based on data and samples from the Pompeia Province that were collected during the Subvent-2 cruise in 2014 aboard the R/V Sarmiento de Gamboa (**Fig. 1**). In order to elucidate the tempo-spatial and genetic relations between CWCs, chemosynthetic fauna and hydrocarbon-rich seepage in this area, we explored geological features (mud volcanoes and coral ridges) by means of underwater imaging and geophysical data. ROV dives were carried out at the Al Gacel MV (D10 and D11) and the Northern Pompeia Coral Ridge (D03). Subsequently, we conducted detailed analyses on selected samples from sites that were characterized by different types of seepage during sampling (**Table 1**). Samples from the Al Gacel MV include authigenic carbonates (D10-R3, D10-R7, D11-R8), pore-water from the sediment (via micro-cores; D10-C5, D10-C8, D11-C10), and water from above the seafloor (via Niskin bottles; D10-N12, D11-N9). Furthermore, a scleractinian coral fragment was recovered from the Northern Pompeia Coral Ridge (D03-B1). All samples were immediately stored at room temperature (petrographic analysis), 4 °C (water, sediments and pore-water analysis), −20 °C (stable isotopic analysis), or −80 °C (environmental DNA analysis).

2.1. Geophysical survey

Seabed topography of the studied sites was mapped by using an Atlas Hydrosweep DS (15 kHz and 320 beams) multibeam echosounder (MBES). Simultaneously, ultra-high resolution sub-bottom profiles were acquired with an Atlas Parasound P-35 parametric chirp profiler (0.5 – 6 kHz). Deep high-resolution multichannel seismic reflection data was obtained using an array of 7 SERCEL gi-guns (system composed of 250 + 150 + 110 + 45 cubic inches) with a total of 860 cubic inches. The obtained data were recorded with an active streamer (SIG®16.3x40.175; 150 m length with 3 sections of 40 hydrophones each). The shot interval was 6 seconds and the recording length 5 seconds two-way travel time (TWT). Data processing (filtering and stacking) was performed on board with Hot Shots software.

2.2. Video survey and analysis

A remotely operated vehicle (ROV-6000 Luso, operated by EMEPC) was used for photographic documentation (high definition digital camera, 1024x1024 pixel) and sampling. The ROV was further equipped with a STD/CTD-SD204 sensor (*in-situ* measurements of salinity, temperature, oxygen, conductivity, sound velocity and depth), HydroC^{TM} sensors (*in-situ* measurements of CO_2 and CH_4), Niskin bottles (CH_4 concentrations, pH and redox potential measurements), and a ROV core sampler (up to 16 cm).

2.2.1. Seawater and pore-water analysis

Niskin water-samples and micro-cores covering the water/sediment interface were recovered from an active pockmark close to the summit of the Al Gacel MV (D10-N4, D10-C5, D10-C8; same site as carbonate-sample D10-R7) as well as directly from its summit (D11-N9, D11-C10). Redox potentials (ORP) and pH-values of the water contained in the Niskin bottles were measured on site with HANNA portable instruments (HI 9025). Pore-water from the micro-cores was immediately extracted by centrifuging 10 cm thick slices of the sediments. Upon extraction, the pore-water was filtered with syringe filters of cellulose acetate (0.2 µm pore), acidified with distilled nitric acid (HNO_3), and stored under 4 °C before further analysis. Major and trace elements were subsequently measured with an Agilent 7500c inductively coupled plasma mass spectrometer (ICP-MS). Method accuracy and precision was checked by external standards (MIV, EPA, NASC, CASS). The precision was better than 5 % RSD (residual standard deviation) and the accuracy better than 4%. Concentrations of S^{2-} were measured with a Hanch-Lange DR 2800 spectrophotometer (cuvette test kit LCK 653).

2.3. Petrographic analysis

General petrographic analysis was performed on thin sections (ca. 60 µm thickness) with a Zeiss SteREO Discovery.V8 stereomicroscope (transmitted- and reflected light) linked to an AxioCam MRc 5-megapixel camera. Additional detailed petrographic analysis of textural and mineralogical features was conducted on polished thin sections (ca. 30 µm thickness) using a DM2700P Leica Microscope coupled to a DFC550 digital camera. Carbonate textures have been classified following Dunham (1962) and Embry & Klovan (1971).

2.4. Stable isotope signatures ($\delta^{13}C$, $\delta^{18}O$) of carbonates

Stable carbon and oxygen isotope measurements were conducted on ca. 0.7 mg carbonate powder obtained with a high precision drill (ø 0.8 mm). The analyses were performed with a Thermo Scientific Kiel IV carbonate device coupled to a Finnigan Delta Plus gas isotope mass spectrometer. Accuracy and reproducibility were checked through the replicate analysis of a standard (NBS19) and reproducibility was better than 0.1 ‰. Stable carbon and oxygen isotope values are expressed in the standard δ notation as per mill (‰) deviations relative to Vienna Pee Dee Belemnite (VPDB).

2.5. Lipid biomarker analysis

2.5.1. Sample preparation

All materials used were pre-combusted (500 °C for >3 h) and/or extensively rinsed with acetone prior to sample contact. A laboratory blank (pre-combusted sea sand) was prepared and analyzed in parallel to monitor laboratory contaminations.

The preparation and extraction of lipid biomarkers was conducted in orientation to descriptions in Birgel et al. (2006). Briefly, the samples were first carefully crushed with a hammer and internal parts were powdered with a pebble mill (Retsch MM 301, Haan, Germany). Hydrochloric acid (HCl; 10 %) was slowly poured on the powdered samples which were covered with dichloromethane (DCM)-cleaned water. After 24 h of reaction, the residues (pH 3 – 5) were repeatedly washed with water and then lyophilized.

3 g of each residue was saponified with potassium hydroxide (KOH; 6 %) in methanol (MeOH). The residues were then extracted with methanol (40 mL, 2x) and, upon treatment with HCl (10 %) to pH 1, in DCM (40 mL, 2x) by using ultra-sonification. The combined supernatants were partitioned in DCM vs. water (3x). The total organic

extracts (TOEs) were dried with sodium sulfate ($NaSO_4$) and evaporated with a gentle stream of N_2 to reduce loss of low-boiling compounds (cf. Ahmed and George, 2004).

Fifty percent of each TOE was separated over a silica gel column (0.7 g Merck silica gel 60 conditioned with *n*-hexane; 1.5 cm i.d., 8 cm length) into (a) hydrocarbon (6 mL *n*-hexane), (b) alcohol (7 mL DCM/acetone, 9:1, v:v) and (c) carboxylic acid fractions (DCM/MeOH, 3:1, v:v). Only the hydrocarbons were subjected to gas chromatography–mass spectrometry (GC-MS).

2.5.2. Gas chromatography–mass spectrometry (GC-MS)

Lipid biomarker analyses of the hydrocarbon fraction were performed with a Thermo Scientific Trace 1310 GC coupled to a Thermo Scientific Quantum XLS Ultra MS. The GC was equipped with a capillary column (Phenomenex Zebron ZB-5MS, 30 m length, 250 µm inner diameter, 0.25 µm film thickness). Fractions were injected into a splitless injector and transferred to the column at 300 °C. The carrier gas was He at a flow rate of 1.5 mL min^{-1}. The GC oven temperature was ramped from 80°C (1 min) to 310 °C at 5 °C min^{-1} (held for 20 min). Electron ionization mass spectra were recorded in full scan mode at an electron energy of 70 eV with a mass range of m/z 50 – 600 and scan time of 0.42 s. Identification of individual compounds was based on comparison of mass spectra and GC retention times with published data and reference compounds.

2.5.3 Gas chromatography–combustion–isotope ratio mass spectrometer (GC-C-IRMS)

Compound specific $\delta^{13}C$ analyses were conducted with a Trace GC coupled to a Delta Plus IRMS via a combustion-interface (all Thermo Scientific). The combustion reactor contained CuO, Ni and Pt and was operated at 940°C. The GC was equipped with two serially linked capillary columns (Agilent DB-5 and DB-1; each 30 m length, 250 µm inner diameter, 0.25 µm film thickness). Fractions were injected into a splitless injector and transferred to the GC column at 290°C. The carrier gas was He at a flow rate of 1.2 ml min^{-1}. The temperature program was identical to the one used for GC-MS (see above). CO_2 with known $\delta^{13}C$ value and a standard (IAEA600) were used for internal calibration. Instrument precision was checked using a mixture of *n*-alkanes with known isotopic composition. Standard deviations of duplicate sample measurements were generally better than 1.0 ‰. Carbon isotope ratios are expressed as $\delta^{13}C$ (‰) relative to VPDB.

2.6. Amplicon sequencing of 16S rRNA genes

2.6.1. DNA extraction and 16S rRNA gene amplification

Environmental DNA analyses of microbial communities were performed on a carbonate sample with embedded corals from the base of the Al Gacel MV (D10-R3), a carbonate sample from an active pockmark close to the summit of the Al Gacel MV (D10-R7), and a necrotic fragment of a living *Madrepora oculata* recovered from the Northern Pompeia Coral Ridge (D03-B1). About 1 – 4 g of solid samples were first mashed with mortar and liquid nitrogen to fine powder. Three biological replicates were used per sample. Total DNA was isolated with a Power Soil DNA Extraction Kit (MO BIO Laboratories, Carlsbad, CA). All steps were performed according to the manufacturer's instructions.

Bacterial amplicons of the V3 – V4 region were generated with the primer set MiSeq_Bacteria_V3_forward primer (5'-TCGTCGGCAGCGTCAGATGTGTATAAGAGACAGCCTACGGGNGGCWGCAG-3') and MiSeq_Bacteria_V4_reverse primer (5'-

GTCTCGTGGGCTCGGAGATGTGTATAAGAGACAGGACTACHVGGGTATCTAATCC-3'). Likewise, archaeal amplicons of the V3 – V4 region were generated with the primer set MiSeq_Archaea_V3_forward primer (5'-TCGTCGGCAGCGTCAGATGTGTATAAGAGACAG-GGTGBCAGCCGCCGCGGTAA-3') and MiSeq_Archaea_V4_reverse primer (5'-GTCTCGTGGGCTCGGAGATGTGTATAAGAGACAG-CCCGCCAATTYCTTTAAG-3'). 50 µl of the PCR reaction mixture for bacterial DNA amplification, contained 1 U Phusion high fidelity DNA polymerase (Biozym Scientific, Oldendorf, Germany), 5% DMSO, 0.2 mM of each primer, 200 µM dNTP, 0.15 µl of 25 mM $MgCl_2$, and 25 ng of isolated DNA. The PCR protocol for bacterial DNA amplification included (i) initial denaturation for 1 min at 98 °C, (ii) 25 cycles of 45 s at 98 °C, 45 s at 60 °C, and 30 s at 72 °C, and (iii) a final extension at 72 °C for 5 min. The PCR reaction mixture for archaeal DNA amplification was similarly prepared but contained instead 1 µl of 25 mM $MgCl_2$ and 50 ng of isolated DNA. The PCR protocol for archaeal DNA amplification included (i) initial denaturation for 1 min at 98 °C, (ii) 10 cycles of 45 s at 98 °C, 45 s at 63 °C, and 30 s at 72 °C, (iii) 15 cycles of 45 s at 98 °C, 45 s at 53 °C, and 30 s at 72 °C, and (iv) a final extension at 72 °C for 5 min.

PCR products were checked by agarose gel electrophoresis and purified using the GeneRead Size Selection Kit (QIAGEN GmbH, Hilden, Germany).

2.6.2. Data analysis and pipeline

Illumina PE sequencing of the amplicons and further process of the sequence data were performed in the Göttingen Genomics Laboratory (Göttingen, Germany). After Illumina MiSeq processing, sequences were analyzed as described in Egelkamp et al. (2017) with minor modifications. In brief, paired-end sequences were merged using PEAR v0.9.10 (Zhang et al., 2014), sequences with an average quality score below 20 and containing unresolved bases were removed with QIIME 1.9.1 (Caporaso et al., 2010). Non-clipped reverse and forward primer sequences were removed by employing cutadapt 1.15 (Martin, 2011). USEARCH version 9.2.64 was used following the UNOISE pipeline (Edgar, 2010). In detail, reads shorter than 380 bp were removed, dereplicated, and denoised with the UNOISE2 algorithm of USEARCH resulting in amplicon sequence variants (ASVs) (Callahan et al., 2017). Additionally, chimeric sequences were removed using UCHIME2 in reference mode against the SILVA SSU database release 132 (Yilmaz et al., 2014). Merged paired-end reads were mapped to chimera-free ASVs and an abundance table was created using USEARCH. Taxonomic classification of ASVs was performed with BLAST against the SILVA database 132. Extrinsic domain ASVs, chloroplasts, and unclassified ASVs were removed from the dataset. Sample comparisons were performed at same surveying effort, utilizing the lowest number of sequences by random subsampling (20,290 reads for bacteria, 13,900 reads for archaea).

The paired-end reads of the 16S rRNA gene sequencing were deposited in the National Center for Biotechnology Information (NCBI) in the Sequence Read Archive SRP156750.

3. Results

3.1. The Pompeia Province — geological settings

The Pompeia Province is situated in the Gulf of Cádiz offshore Morocco, within the so-called Middle Moroccan Field (Ivanov et al., 2000) at water-depths between 860 and 1000 m (**Fig. 1**). It encompasses the active Al Gacel MV (**Fig. 1, C**), another mud volcano which is extinct (further referred as extinct MV) and two east-west elongated ridges (Northern Pompeia Coral Ridge and Southern Pompeia Coral Ridge). CWCs occur on all of these

morphological features and scattered coral-mounds surround the ridges with a smooth relief (**Fig. 1, B**). Detailed geological profiles and 3D images of these features are shown in **Figs. 2** and **3**.

The Al Gacel MV is a cone-shape structure, 107 m high and 944 m wide, with its summit at 762 m depth and surrounded by a 11 m deep rimmed depression (León et al., 2012) (**Fig. 1, C**). It is directly adjacent to the Northern Pompeia Coral Ridge (**Fig. 2, A–B**), which extends ca. 4 km in westward direction (**Fig. 2, A–B**) and it is terminated by the Pompeia Escarpment (**Fig. 1, B; Fig. 2, C**). High resolution seismic profiles of the Pompeia Escarpment show CWC build-ups (R1 to R4) with steep lateral scarps of ca. 40 m height (**Fig. 2, C**). The Al Gacel MV is of sub-circular shape and exhibits a crater at its top (**Fig. 2, A–B**).

Ultra-high resolution sub-bottom seismic profile crossing the Pompeia Province from northwest (NW) to southeast (SE) (**Fig. 3, A**), shows (i) the Al Gacel MV surrounded by bottom-current deposits, (ii) an up to 130 m high CWC framework, growing on top the Southern Pompeia Coral Ridge, and (iii) semi-buried CWC mounds surrounding the ridge in areas of low relief. These CWC mounds locally form smooth, up to 25 – 30 m high topographic reliefs that are exposed, but then taper downward below the seafloor (applying sound speeds of 1750 m/s in recent sediments). Additionally, a multichannel seismic profile following the same track but with higher penetration below the seafloor (**Fig. 3, B**) shows high amplitude reflections inside the Al Gacel cone and enhanced reflections at the top of the diapirs (yellow dotted-line in **Fig. 3, B**), pointing to the occurrence of gas (hydrocarbon)-charged sediments. It furthermore exhibits breaks in seismic continuity and diapiric structures at different depths below the Southern Pompeia Coral Ridge and the Al Gacel MV, evidencing the presence of a fault system (**Fig. 3, B**). These tectonic structures may promote the development of overpressure areas (OP in **Fig. 3, B**) and consequent upward fluid flow to the surface.

3.2. ROV observation and measurements

Submersible ROV surveys at the Al Gacel MV (**Fig. 1, C**) revealed the presence of dispersed pockmark depressions at the eastern (Dive 10, 790 m) and northern flanks (Dive 11, 760 – 825 m depth). These sites are characterized by focused but low intensity seafloor bubbling (e.g. **Fig. 4, B**; **Fig. 5, A**). Analysis of water samples revealed CH_4-concentration up to 171 nM during Dive 10 and up to 192 nM during Dive 11 (Sánchez-Guillamón et al., 2015).

Pockmarks are typically characterized by grey-olive mud breccia sediments and authigenic carbonates, appearing in the center and edges. The authigenic carbonates are commonly assocaited with typical methane-seep related organisms (e.g. sulfide-oxidizing bacterial mats, chemosynthetic bivalves, siboglinid tubeworms) (**Fig. 4, B–C**; **Fig. 5**). Communities of non-chemosynthetic organisms (e.g. sponges, corals) were also found at pockmarks (**Fig. 4, B–C**; **Fig. 5, C**), but were more abundant in places where no seepage was detected (**Fig. 4, A**).

Observations with the submersible ROV at the Northern Pompeia Coral Ridge and the extinct MV (Dive 03) revealed widespread and abundant occurrences of dead scleractinian-corals (mainly *Madrepora oculata* and *Lophelia pertusa*) currently colonized by few living non-chemosynthetic organisms (e.g. *Corallium tricolor*, other octocorals, sea urchins) (**Fig. 6, B–D**). Locally, grey-black colored patches of sulfide-oxidizing bacterial mats surrounded by dead chemosynthetic bivalves (*Lucinoma asapheus* and *Thysira vulcolutre*) were observed (**Fig. 6, A**). CH_4-seepage appeared to be less than at the Al Gacel MV, with concentrations of 80 – 83 nM.

Water parameters display homogenous values between the four sampling sites (10 °C temperature, ca. 52 – 55 % dissolved oxygen, ca. 31 Kg/m^3 density) (**Table 2**). At depths of 790 m (D10-N4, same site as carbonate D10-R7) and 760 m (D11-N9), the pH of seawater was 7.88 and 7.85, respectively (**Table 3**). The same seawater samples

exhibited ORP values of 136 mV (D10-N4) and 257 mV (D11-N9) (**Table 3**). Further analysis of these seawater samples revealed Fe^{2+} concentration of 0.57 and 0.31 µM, while S^{2-} values were nearly absent (below detection limit) (**Table 2**). Fe^{2+} concentrations in pore-waters ranged between 0.94 – 1.27 µM (D10-C5), 2.70 – 1.74 µM (D10-C8), and 2.39 – 5.32 µM (D11-C10). S^{2-} concentrations in pore-waters were below detection limit (D10-C5), 50.23 µM (D10-C8), and 0.47 µM (D11-C10) (**Table 3**).

3.3. Petrography and stable isotopes signatures of carbonates ($\delta^{18}O$, $\delta^{13}C$)

Sample D10-R3 derives from a field of carbonates at the base of the Al Gacel MV which is inhabited by sponges and corals (**Fig. 4, A**). The sample is a framestone composed of deep water scleractinian corals (*Madrepora* and rare *Lophelia*) (**Fig. 7, A–B**). The corals are typically cemented by microbial automicrite (*sensu* Reitner et al. 1995) followed by multiple generations of aragonite. A matrix of dark allomicrite (*sensu* Reitner et al. 1995) with oxidized framboidal pyrites and remains of planktonic foraminifera is restricted to few bioerosional cavities (ca. 5%) in the skeletons of dead corals (**Fig. 8, A–B**). $\delta^{13}C$ signatures of the matrix and cements range from −26.68 to −18.38 ‰, while the embedded coral fragments exhibit $\delta^{13}C$ values between −5.58 and −2.09 ‰ (**Fig. 7, B; Table 4**). The $\delta^{18}O$ values generally range from +2.35 to +3.92 ‰ (**Fig. 9; Table 4**).

Sample D10-R7 was recovered from a pockmark on the eastern site of the Al Gacel MV that is virtually influenced by active seepage (**Fig. 3, C**). It consists of black carbonate and exhibits a strong hydrogen sulfide (H_2S) odor (**Fig. 5, B**; **Fig. 7, C–D**). The top of this sample was inhabited by living octocorals (**Fig. 5, C)**, while chemosymbiotic siboglinid worms were present on the lower surface (**Fig. 5, D**). The sample is characterized by a grey peloidal wackestone texture consisting of allomicrite with abundant planktonic foraminifers and few deep water miliolids. The sample furthermore exhibits some fractured areas which are partly filled by granular and small fibrous cement, probably consisting of Mg-calcite. Locally, light brownish crusts of microbial automicrite similar to ones in D10-R3 are present (see above). Framboidal pyrite is abundant and often arranged in aggregates (**Fig. 8, C–D**). The carbonate exhibits $\delta^{13}C$ values ranging from −28.77 to −21.13 ‰ and $\delta^{18}O$ values from +2.37 to +3.15 ‰ (**Fig. 9; Table 4**).

Sample D11-R8 comes from an area with meter-sized carbonate blocks at the summit of the Al Gacel MV and is mainly colonized by sponges and serpulid worms (**Fig. 4, D**). The sample generally exhibits a light grey mud- to wackestone texture consisting of allomicrite with few scleractinian-coral fragments and planktonic foraminifers (**Fig. 7, E–F**). The carbonate furthermore contains abundant quartz silt and, locally, pyrite enrichments. A further prominent feature are voids that are encircled by dark grey halos and exhibit brownish margins (due to enrichments of very small pyrite crystals and organic matter, respectively). $\delta^{13}C$ signatures of the matrix and cements range from −14.82 to −14.74 ‰, while embedded coral fragments exhibit $\delta^{13}C$ values of −4.91 to −2.99 ‰ (**Fig. 7, F; Table 4**). $\delta^{18}O$ values generally range from +1.49 to +5.60 ‰ (**Fig. 9; Table 4**).

Sample D03-B1 is a necrotic fragment of a living scleractinian coral (*Madrepora oculata*) recovered from the Northern Pompeia Coral Ridge (**Fig. 6, D**; **Fig. 7, G**). The coral-carbonate exhibits $\delta^{13}C$ values ranging from −8.08 to −1.39 ‰ and $\delta^{18}O$ values from −0.31 to +2.26 ‰ (**Fig. 9**; **Table 4**).

3.4. Lipid biomarkers and compound specific carbon isotope signatures

The hydrocarbon fractions of the carbonate recovered from the active pockmark (D10-R7) mainly consist of the irregular, tail-to-tail linked acyclic isoprenoids 2,6,11,15-tetramethylhexadecane (C_{20}; crocetane), 2,6,10,15,19-

pentamethylicosane (C_{25}; PMI), as well as of several unsaturated homologues of these compounds (**Fig. 10**). Additionally, it contains the regular, head-to-tail linked acyclic isoprenoid pristane (C_{19}).

The hydrocarbon fraction of the carbonate recovered from the summit of the Al Gacel MV (D11-R8) is dominated by *n*-alkanes with chain-lengths ranging from C_{14} to C_{33} (maxima at *n*-C_{16} and, subordinated, at *n*-C_{20} and *n*-C_{31}) (**Fig. 10**). The sample further contains pristane, a mixture of crocetane and the head-to-tail linked acyclic isoprenoid phytane (C_{20}) (co-eluting), as well as traces of PMI.

In the carbonate from the active pockmark (D10-R7), crocetane and PMI exhibited strongly depleted $\delta^{13}C$ values (−101.2 ‰ and −102.9 ‰, respectively). In the carbonate from the summit of the volcano (D11-R8), crocetane/phytane and PMI showed less depleted $\delta^{13}C$ values (−57.2 ‰ and −74.3 ‰, respectively). $\delta^{13}C$ values of *n*-alkanes in the carbonate D11-R8 (*n*-C_{17-22}) ranged between −30.8 ‰ and −33.0 ‰ (**Table 5**).

3.5. DNA inventories (MiSeq Illumina sequences)

Bacterial DNA from samples D10-R3 (authigenic carbonate, base of the Al Gacel MV) and D03-B1 (*Madrepora oculata* fragment, Northern Pompeia Coral Ridge) mainly derives from taxa that typically thrive in the water-column (e. g. Actinobacteria, Acidobacteria, Chloroflexi, Bacteroidetes, Woeseiaceae, Dadabacteria, Kaiserbacteria, Poribacteria, Planctomycetes, Gemmatimonadetes) (**Fig. 11, A**). The sample D10-R3 furthermore contains bacterial DNA of the nitrite-oxidizing bacteria *Nitrospira sp.*, while the sample D03-B1 contains DNA of the bacterial taxa Verrucomicrobia, Enterobacteria, and *Nitrosococcus*. Noteworthy, one amplicon sequence variant (ASV_189) with low number of clustered sequences has been found in D03-B1, identified as a methanotrophic symbiont of *Bathymodiolus mauritanicus* (see Rodrigues et al., 2013).

Up to 50 % of bacterial DNA in sample D10-R7 (authigenic carbonate, top of the Al Gacel MV) derives from taxa that are commonly associated with fluid seepage and AOM, i.e. sulfide-oxidizing bacteria, sulfate-reducing bacteria (SRB) and methane-oxidizing bacteria. The most abundant are SRB taxa like SEEP-SRB1, SEEP-SRB2, *Desulfatiglans*, *Desulfobulbus* and *Desulfococcus*, which typically form consortia with ANME archaea.

Archaeal DNA (**Fig. 11, B**) from samples D10-R3 and D03-B1 mainly consist of *Cenarchaeum sp.*, which represents 70 – 90 %. *Candidatus Nitrosopumilus* is the second most abundant in both samples, representing 5 – 20 %. In contrast, around 90 % of archaeal DNA in D10-R7 is related to ANME-1 and ANME-2 groups, in good concordance with the relative abundances of SRB DNA.

Details of the number of reads per taxa are shown in the supplementary data, **Tables 1** and **2**.

4. Discussion

4.1. Evidence for hydrocarbon-rich seepage affecting the Pompeia Province

Two-dimensional multichannel-seismic images show that the Pompeia Province is affected by fluid expulsion related to compressional diapiric ridges and thrust faults (**Fig. 3, B**), as it has been reported from other areas of the Gulf of Cádiz (Somoza et al., 2003; Van Rensbergen et al., 2005; Medialdea et al., 2009). There seem to be different types of fault-conduit systems that link the overpressure zones (OP) with the seafloor (**Fig. 3, B**), controlling both the type and rate of seepage (e.g. eruptive, focused, diffused or intermittent, the latter referred to as “dripping-like” in the following). At the Al Gacel MV, conduits are for instance mainly linked to faults and a dense hydro-fracture network, allowing the migration of hydrocarbon-rich muds from the overpressure zone to the surface. During active episodes, eruptions lead to the formation of mud-breccia flows as observed in gravity cores

(e.g. León et al., 2012). During rather dormant episodes, focused and dripping-like seepage predominates, forming pockmark features (**Fig. 4, B**).

Currently, the Al Gacel MV is affected by continuous and focused dripping-like seepages. These sites of active seepage are characterized by carbonates that are suspected to be methane-derived (e.g. sample D10-R7, **Fig. 4, B–C**). In-situ ROV-measurements and subsequent water sample analysis demonstrated high concentrations of CH_4 in fluids that were escaping upon removal of the carbonate D10-R7 from the active pockmark (171 nM; **Fig. 5, A**) (Sánchez-Guillamón et al., 2015). This association suggests a genetic relationship between hydrocarbon-rich seepage and the carbonate, as also reflected low $\delta^{13}C$-signatures of the carbonates analyzed herein (down to ca. −30 ‰, **Fig. 9; Table 3**). Indeed, the grey peloidal texture of this sample resembles that of AOM-derived automicrites from the Black Sea that are related to micro-seepage of methane (cf. Reitner et al., 2005). The here observed isotopically depleted acyclic isoprenoids such as crocetane and PMI ($\delta^{13}C$ values between ca. −103 and −57‰; **Fig. 10; Table 4**) are typical fingerprints of AOM-associated Archaea (Hinrichs et al., 1999; Thiel et al., 1999, 2001; Peckmann et al., 2001; Peckmann & Thiel, 2004), which is also in good accordance with the high abundance of DNA related to ANME. At the same time, elevated concentrations of S^{2-} and Fe^{2+} in pore-waters of D10-C8 micro-core (0.23 µM and 1.74 µM, respectively; **Table 2**), abundant framboidal pyrite (**Fig. 8, C–D**) and SRB-related DNA in the carbonate (**Fig. 11**) evidence microbial sulfate reduction in the environment. All these data clearly demonstrate that the carbonates have been formed via AOM, fueled by fluids from the underlying mud diapir.

Other carbonate samples from the Al Gacel MV (i.e. D10-R3 and D11-R8) probably have also been formed due to AOM as they are isotopically depleted as well ($\delta^{13}C$ values between ca. −25 and −15 ‰, **Fig. 9**, **Table 3**). However, no active gas bubbling was observed during sampling, even though both samples still contain open voids which could form pathways for fluids. Several characteristics of these voids (e.g. dark halos formed by pyrite, brownish margins due to organic matter enrichments) are very similar to those of methane-derived carbonate conduits (cf. Reitner et al., 2015). This could imply that the intensity of hydrocarbon-rich seepage and consequently AOM, may have fluctuated through time. This in good accordance with the relatively low dominance of crocetane and PMI in a carbonate sampled from the summit of Al Gacel MV (D11-R8; **Fig. 10**). The moderately depleted $\delta^{13}C$ values of crocetane/phytane and PMI in this sample (−57.2 ‰ and −74.3 ‰, respectively; **Table 4**) could be due to mixing effects and are thus also in agreement with varying intensities of AOM in the environment. The presence of only few AOM-related DNA sequences (**Fig. 11**) and partly oxidized pyrites in the carbonate D10-R3 from the base of the Al Gacel MV (**Fig. 8, A–B**) are well in line with this scenario.

There is no evidence for eruptive extrusions of muddy materials at the coral ridges. In the Southern Pompeia Coral Ridge (**Fig. 3**), diapirs appear to rather promote an upward migration of hydrocarbon-rich fluids in a divergent way throughout a more extensive seabed area. This results in a continuous and diffused seepage, which promotes the occurrence of AOM and the formation of MDACs at the base of the ridges, related to the sulphate-methane transition zone (SMTZ) (Boetius et al., 2000; Hinrichs and Boetius, 2002; González et al., 2012a). This is in good accordance with the detection of methane (80 – 83 nM) at the Northern Pompeia Coral Ridge and the presence of sulfide-oxidizing bacterial mats and shells of dead chemosynthetic bivalves at the western part of the ridge (**Fig. 6, A**). Likewise, the CWC Mounds Field surrounding the Southern Pompeia Coral Ridge (**Fig. 3**) is thoroughly characterized by micro-seeps, due to ascending fluids from OPs through low-angle faults. This type of focused seepage may promote formation of MDAC pavements in deeper layers of the sediments (**Fig. 3**), similar to coral

ridges along the Pen Duick Escarpment (Wehrmann et al., 2011). The generation of MDAC-hotspots at sites of such seepage also explain the geometry of the downward tapering cones (**Fig. 3**).

4.2. Ecological meaning of hydrocarbon-rich seepage for CWCs

Our data suggests contemporaneous micro-seepage and CWC growth in the Pompeia Province (e.g. **Fig. 4, B**). This relationship has also been observed elsewhere, e.g. in the North Sea and off Mid Norway (Hovland, 1990; Hovland & Thomsen, 1997), and the Angola margin (Le Guilloux et al., 2009). Corals utilize HCO_3^- deriving from both the environment and the internal production of CO_2 for skeleton biomineralization (Swart, 1983; Zoccola et al., 2015; Nakamura et al., 2018). Hence, a potential utilization of methane as a carbon source should be reflected in the $\delta^{13}C$ signatures of their skeletons. However, scleractinian fragments recovered from the Al Gacel MV (embedded in carbonates D10-R3 and D11-R8, from the base and summit of the volcano, respectively) and the Northern Pompeia Coral Ridge (D03-B1, necrotic part of a living *Madrepora oculata*) displayed barely depleted $\delta^{13}C$ values (ca. −8 to −1 ‰; **Fig. 9**; **Table 3**), close to the $\delta^{13}C$ of marine seawater (0 ± 3 ‰, e.g. Hoefs, 2015). These values do not support a significant uptake of methane-derived carbon by the CWCs and thus a direct trophic dependency as previously proposed (Hovland, 1990). Furthermore, the only DNA in sample D03-B1 that could be attributed to a potential methanotrophic endosymbiont (ASV_189: Rodrigues et al., 2013) occurred in minor amounts and most likely represents contamination from the environment or during sampling. It appears therefore more likely that the CWCs feed on a mixture of phytoplankton, zooplankton and dissolved organic matter as previously proposed for ones in other regions (Kiriakoulakis et al., 2005; Duineveld et al., 2007; Becker et al., 2009; Liebetrau et al., 2010). This is in good accordance with the presence of DNA from various common archaeal and bacterial taxa (e.g. Acidobacteria, Actinobacteria, Candidatus *Nitrosopumilus*, *Cenarchaeum sp.*) and some potential members of the corals' holobiont (e.g. Enterobacteria, Verrucomicrobia, *Nitrosococcus sp.*) (Sorokin, 1995; Rädecker et al., 2015; Webster et al., 2016) in sample D03-B1 (**Fig. 11**). Taken together, there is no evidence that CWCs in the working area harbor microbial symbionts which potentially could utilize the hydrocarbon-rich fluids. However, future analyses on living coral-tissue will be important to verify this conclusion.

CWC development and hydrocarbon-rich seepage appear to be rather linked *via* the formation of MDAC deposits, which provide the hard substrata needed for CWC larval settlement (e.g. Díaz-del-Rio et al., 2003; Van Rooij et al., 2011; Magalhães et al., 2012; Le Bris et al., 2016; Rueda et al., 2016). If too severe, however, fluid flow and associated metabolic processes can result in local conditions that are lethal to CWCs (see 4.3). Moreover, AOM fueled by fluid flow can also cause an entombment of the CWCs by MDACs (Wienberg et al., 2009, Wienberg & Titschack, 2015), as observed in D10-R3 and D11-R8 carbonates from the Al Gacel MV (**Figs. 7 and 9**; **Tables 3 and 4**). It is therefore not surprising that large CWC systems in the Pompeia Province are always linked to structures that are affected by rather mild, non-eruptive seepage (i.e. the extinct MV, the coral ridges and the CWC Mound Fields: **Figs. 3 and 6**). The observation that these systems are in large parts "coral graveyards" (**Fig. 6, B–D**), similar to other areas in the Gulf of Cádiz (see Foubert et al., 2008; Wienberg et al., 2009), may be explained by a post-glacial decrease in current strength (Foubert et al., 2008). In the light of our findings, however, they could also have been negatively affected by periods of intensive seepage during higher tectonic activity. Future studies are important to test this hypothesis in greater detail.

4.3. Spatio-temporal co-existence of CWCs and chemosynthetic organisms — the buffer effect

As discussed above, MDAC deposits are ecologically beneficial for CWCs, as they serve as optimal substrata even when seepage is still present (e. g. Hovland, 1990; Hovland & Thomsen, 1997; Le Guilloux et al., 2009; this study). Severe hydrocarbon-rich seepage, however, is ecologically stressful for the corals. Particularly, fluid- and AOM-derived hydrogen sulfide is considered problematic because of its role in coral necrosis (Myers & Richardson, 2009; García et al., 2016) and carbonate dissolution effects (Wehrmann et al., 2011). Corals appear to be physiologically tolerant to various of these environmental stressors such as low oxygen concentrations and acidification (e. g. Dodds et al., 2007; Form & Riebesell, 2012; McCulloch et al., 2012; Movilla et al., 2014). Hydrogen sulfides can furthermore efficiently be buffered through the reaction with Fe-(oxyhydro)-oxides or Fe^{2+} dissolved in pore waters, ultimately forming pyrite (Wehrmann et al., 2011). It appears that the combination of these ecological capabilities plus certain environmental factors allows CWCs to thrive in areas affected by hydrocarbon seepage. Fe-(oxyhydro)-oxides nodules have previously been observed in the Iberian and Moroccan margins (González et al., 2009; 2012b), but not in the Pompeia Province. Instead, sulfide-oxidizing bacteria living in symbiosis with invertebrates (e.g. siboglinid worms: Petersen & Dubilier, 2009) (**Fig. 5, D**) and thriving in mats (**Fig. 4, C**; **Fig. 6, A**) were particularly prominent. These microbes withdraw reduced sulfur species through their metabolic activity, thus forming a biological buffer. Likewise, microbially mediated AOM substantially increases carbonate alkalinity at active sites, thereby providing a buffer against acidification on a local scale (e. g., in the active pockmark from the Al Gacel MV where seawater pH was 7.85, see section 3.2). We propose that such biological buffers provide a further ecological linkage between hydrocarbon-rich seepage and cold-water corals along the Pompeia Province ("buffer effect model": **Fig. 12**). The impact and exact capacity of this biological buffer, however, remains elusive and must be evaluated in future studies.

5. Conclusions

Cold-water coral occurrences in the Pompeia Province (Gulf of Cádiz) are typically linked to hydrocarbon-seep structures like mud volcanoes and diapirs. The irregular topography of these structures affects bottom water-currents which supply nutrients to the corals. A further ecological benefit is the seepage-fueled formation of authigenic carbonates, which provide ideal substrates for coral larvae settlement. Cold-water corals therefore take indirectly advantages of seepage-related conditions, instead of feeding from the seeped fluids, such as sulfide and methane. However, increased fluid seepage appears to be ecologically disadvantageous as evidenced by corals embedded in some of the carbonates. Consequently, cold-water coral growth in these habitats depends directly on seepage intensity and how these fluids are drained onto the seafloor (i.e. eruptive, focused, diffused or dripping-like). Cold-water coral growth appears to be furthermore supported by the microbial-mediated removal of seepage-related toxic substances (e. g., reduced sulfur species through sulfide-oxidizing bacteria) and shaping of environmental conditions (e. g., pH-buffering through AOM). This biological buffer is possibly crucial to keep conditions favorable for the growth of cold-water corals in the studied area, particularly in times of increased fluid seepage.

Author contribution

Blanca Rincón-Tomás, Dominik Schneider and Michael Hoppert carried out the microbial analysis. Jan-Peter Duda carried out the biomarker analysis. Luis Somoza and Teresa Medialdea processed seismic and bathymetric data. Pedro Madureira processed ROV data. Javier González and Joachim Reitner carried out the petrographic

analysis. Esther Santofimia and Enrique López-Pamo carried out the pore-water and seawater analysis. Joachim Reitner carried out the stable isotopic analysis. Blanca Rincón-Tomás prepared the manuscript with contributions from all co-authors.

Competing interests

The authors declare that they have no conflict of interest.

Acknowledgments

The authors thank the captain and the crew on board the R/V Sarmiento de Gamboa, as well as the UTM (Unidad de Tecnología Marina), that have been essential for the success of this paper. Data obtained on board is collected in the SUBVENT-2 cruise, which can be found in the IGME archive. This work was supported by the Spanish project SUBVENT (CGL2012-39524-C02) and the project EXPLOSEA (CTM2016-75947) funded by the Spanish Ministry of Science, Innovation and Universities.

References

Ahmed, M. and George, S.C.: Changes in the molecular composition of crude oils during their preparation for GC and GC–MS analyses, Org. Geochem., 35, 137–155, doi:10.1016/j.orggeochem.2003.10.002, 2004.

Becker, E. L., Cordes, E. E., Macko, S. A., and Fisher, C. R.: Importance of seep primary production to *Lophelia pertusa* and associated fauna in the Gulf of Mexico, Deep-sea Res Pt I, 56(5), 786–800, doi:10.1016/j.dsr.2008.12.006, 2009.

Birgel, D., Thiel, V., Hinrichs, K. U., Elvert, M., Campbell, K. A., Reitner, J., Farmer, J. D., and Peckmann, J.: Lipid biomarker patterns of methane-seep microbialites from the Mesozoic convergent margin of California, Org. Geochem., 37(10), 1289–1302, doi:10.1016/j.orggeochem.2006.02.004, 2006.

Boetius, A., Ravenschlag, K., Schubert, C. J., Rickert, D., Widdel, F., Gieseke, A., Amann, R., Jørgensen, B. B., Witte, U., and Pfannkuche, O.: A marine microbial consortium apparently mediating anaerobic oxidation of methane, Nature, 407 (6804), 623–626, doi:10.1038/35036572, 2000.

Callahan, B., MacMurdie, P. J., and Holmes, S. O.: Exact sequence variants should replace optional taxonomic units in marker-gene data analysis, ISME J., 11, 2639–2643, doi:10.1038/ismej.2017.119, 2017.

Caporaso, J.G., Kuczynski, J., Stombaugh, J., Bittinger, K., Bushman, F.D., Costello, E.K., Fierer, N., González-Peña, A., Goodrich, J. K., Gordon, J. I., Huttley, G. A., Knights, D., Koenig, J. E., Lozupone, C. A., McDonald, D., Muegge, B. D., Pirrung, M., Reeder, J., Sevinsky, J. R., Turnbaugh, P. J., Walters, W. A., Widmann, J., Yatsunenko, T., Zaneveld, J., and Knight, R.: QIIME allows analysis of high-throughput community sequencing data, Nat. Methods, 7, 335–336, doi:10.1038/nmeth.f.303, 2010.

Cordes, E., Arnaud-Haond, S., Bergstad, O., da Costa Falcão, A. P., Freiwald, A., Roberts, J. M., and Bernal, P.: Cold water corals, in: The First Global Integrated Marine Assessment, World Ocean Assessment I, United Nations, Cambridge University Press, Cambridge, United Kingdom, 2016.

Díaz-del-Río, V., Somoza, L., Martínez-Frías, J., Mata, M. P., Delgado, A., Hernandez-Molina, F. J., …, Vázquez, J. T.: Vast fields of hydrocarbon-derived carbonate chimneys related to the accretionary

497 wedge/olistostrome of the Gulf of Cádiz, Mar. Geol., 195, 177–200, doi:10.1016/S0025-3227(02)00687-
498 4, 2003.
499 Dodds, L. A., Roberts, J. M., Taylor, A. C., and Marubini, F.: Metabolic tolerance of the cold-water coral *Lophelia*
500 *pertusa* (Scleractinia) to temperature and dissolved oxygen change, J. Exp. Mar. Biol. Ecol., 349(2), 205–
501 214, doi:10.1016/j.jembe.2007.05.013, 2007.
502 Dorschel, B., Hebbeln, D., Foubert, A., White, M., and Wheeler, A. J.: Hydrodynamics and cold-water coral facies
503 distribution related to recent sedimentary processes at Galway Mound west of Ireland, Mar. Geol., 244,
504 184–195, doi:10.1016/j.margeo.2007.06.010, 2007.
505 Duineveld, G. C., Lavaleye, M. S., Bergman, M. J., De Stigter, H., and Mienis, F.: Trophic structure of a cold-
506 water coral mound community (Rockall Bank, NE Atlantic) in relation to the near-bottom particle supply
507 and current regime, B. Mar. Sci., 81 (3), 449–467, 2007.
508 Dullo, W. C., Flögel, S., and Rüggerberg, A.: Cold-water coral growth in relation to the hydrography of the Celtic
509 and Nordic European continental margin, Mar. Ecol. Prog. Ser., 371, 165–176, doi:10.3354/meps07623,
510 2008.
511 Dunham, R. J., 1962, Classification of carbonate rocks according to their depositional texture, in: Classification
512 of Carbonate Rocks, Ham, W. E. (Eds.), American Association of Petroleum Geologists Memoir 1, Tulsa,
513 OK, 108–121, 1962.
514 Edgar, R. C.: USEARCH. http://www.drive5.com/usearch. 2010.
515 Egelkamp, R., Schneider, D., Hertel, R., and, Daniel, R.: Nitrile-Degrading Bacteria Isolated from Compost, Front.
516 Environ. Sci., 5, doi: 10.3389/fenvs.2017.00056, 2017.
517 Embry III, A. F., and Klovan, J. E.: A late Devonian reef tract on northeastern Banks Island, NWT, B. Can. Petrol.
518 Geol., 19(4), 730–781, 1971.
519 Form, A. U., and Riebesell, U.: Acclimation to ocean acidification during long-term CO2 exposure in the cold-
520 water coral *Lophelia pertusa*, Glob, Change Biol., 18(3), 843–853, doi: 10.1111/j.1365-
521 2486.2011.02583.x, 2012.
522 Foubert, A., Depreiter, D., Beck, T., Maignien, L., Pannemans, B., Frank. N., Blamart, D., and Henriet, J.:
523 Carbonate mounds in a mud volcano province off north-west Morocco: key to processes and controls,
524 Mar. Geol., 248, 74–96, doi: 10.1016/j.margeo.2007.10.012, 2008.
525 Garcia, G. D., Santos, E. D. O., Sousa, G. V., Zingali, R. B., Thompson, C. C., and Thompson, F. L.:
526 Metaproteomics reveals metabolic transitions between healthy and diseased stony coral *Mussismilia*
527 *braziliensis*, Mol. Ecol., 25(18), 4632–4644, doi:10.1111/mec.13775, 2016.
528 Goedert, J. L., and Peckmann, J.: Corals from deep-water methane-seep deposits in Paleogene strata of Western
529 Oregon and Washington, U.S.A., in: Cold-water corals and Ecosystems, Freiwald, A., and Roberts, J. M.
530 (eds.), Springer-Verlag, Berlin Heidelberg, 27–40, 2005.
531 Gomes-Sumida, P.Y., Yoshinaga, M.Y., Saint-Pastous Madureira, L.A., and Hovland, M.: Seabed pockmarks
532 associated with deep water corals off SE Brazilian continental slope, Santos Basin, Mar. Geol., 207, 159–
533 167, doi:10.1016/j.margeo.2004.03.006, 2004.
534 González, F. J., Somoza, L., Lunar, R., Martínez-Frías, J., Martín Rubí, J. A., Torres, T., Ortiz, J. E., Díaz-del-
535 Río, V., Pinheiro, L. M., and Magalhães, V. H.: Hydrocarbon-derived ferromanganese nodules in
536 carbonate mud mounds from the Gulf of Cádiz: mud-breccia sediments and clasts as nucleation sites,
537 Mar. Geol., 261, 64–81, doi:10.1016/j.margeo.2008.11.005, 2009.

González, F. J., Somoza, L., León, R., Medialdea, T., de Torres, T., Ortiz, J. E., Martínez-Frías, J., and Merinero, R.: Ferromanganese nodules and micro-hardgrounds associated with the Cádiz Contourite Channel (NE Atlantic): Palaeoenvironmental records of fluid venting and bottom currents, Chem. Geol., 310–311, 56–78, doi: 10.1016/j.chemgeo.2012.03.030, 2012a.

González, F. J., Somoza, L., Medialdea, T., León, R., Torres, T., Ortiz, J. E., and Martín-Rubí, J. A.: Discovery of ferromanganese hydrocarbon-related nodules associated with the Meknes mud volcano (Western Moroccan margin). European Geoscience Union 2012 (EGU2012). Viena (Austria). Geophys. Res. Abs. vol. 14, EGU2012-12306, 2012b.

Hebbeln, D., Van Rooij, D., and Wienberg, C.: Good neighbours shaped by vigorous currents: cold-water coral mounds and contourites in the North Atlantic, Mar. Geol, 378, 171–185, doi:10.1016/j.margeo.2016.01.014, 2016.

Hensen, C., Nuzzo, M., Hornibrook, E., Pinheiro, L.M., Bock, B., Magalhães, V.H., and Brückmann, W.: Sources of mud volcano fluids in the Gulf of Cádiz — indications for hydrothermal imprint, Geochim. Cosmochim. Ac., 71 (5), 1232–1248, doi:10.1016/j.gca.2006.11.022, 2007.

Hinrichs, K. -U., and Boetius, A.: The anaerobic oxidation of methane: new insights in microbial ecology and biogeochemistry, in: Ocean Margin Systems, Wefer, G., Billett, D., Hebbeln, D., Jørgensen, B.B., Schlueter, M., Van Weering, T. (Eds.), Springer-Verlag, Berlin, 457–477, 2002.

Hinrichs, K. -U., Hayes, J. M., Sylva, S. P., Brewer, P. G., and De Long, E. F.: Methane-consuming archaebacteria in marine sediments, Nature, 398, 802–805, doi:10.1038/19751, 1999.

Hoefs, J.: Stable Isotope Geochemistry, Springer, Berlin, 2015.

Hovland, M.: Do carbonate reefs form due to fluid seepage?, Terra Nova, 2, 8–18, doi:10.1111/j.1365-3121.1990.tb00031.x, 1990.

Hovland, M., Jensen, S., and Indreien, T.: Unit pockmarks associated with *Lophelia* coral reefs off mid-Norway: more evidence of control by 'fertilizing' bottom currents, Geo-Mar. Lett., 32 (5–6), 545–554, doi:10.1007/s00367-012-0284-0, 2012.

Hovland, M., Mortensen, P. B., Brattegard, T., Strass, P., and Rokoengen, K.: Ahermatypic coral banks off mid-Norway: evidence for a link with seepage of light hydrocarbons, Palaios, 13, 189–200, doi:10.1043/0883-1351(1998)013<0189:ACBOME>2.0.CO;2, 1998.

Hovland, M., and Thomsen, E.: Cold-water corals — are they hydrocarbon seep related?, Mar. Geol., 137, 159–164, doi:10.1016/S0025-3227(96)00086-2, 1997.

Huvenne, V. A., Masson, D. G., and Wheeler, A. J.: Sediment dynamics of a sandy contourite: the sedimentary context of the Darwin cold-water coral mounds, Northern Rockall Trough, Int. J. Earth Sci., 98 (4), 865–884, doi: 10.1007/s00531-008-0312-5, 2009.

Ivanov, M. K., Akhmetzhanov, A. M., and Akhmanov, G. G.: Multidisciplinary study of geological processes on the North East Atlantic and Western Mediterranean Margins, in: Ioc. Tech. S., 56, UNESCO, 2000.

Kiriakoulakis, K., Fisher, E., Wolff, G. A., Freiwald, A., Grehan, A., and Roberts, J. M.: Lipids and nitrogen isotopes of two deep-water corals from the North-East Atlantic: initial results and implications for their nutrition, in: Cold-Water Corals and Ecosystems, Freiwald, A., Roberts, J. M. (Eds.), Erlangen Earth Conf., Springer, Germany, 715–729, 2005.

Le Bris, N., Arnaud-Haond, S., Beaulieu, S., Cordes, E. E., Hilario, A., Rogers, A., van de Gaever, S., and Watanabe, H.: Hydrothermal Vents and Cold Seeps, in: The First Global Integrated Marine Assessment, United Nations, Cambridge University Press, Cambridge, United Kingdom, 2016.

Le Guilloux, E., Olu, K., Bourillet, J. F., Savoye, B., Iglésias, S. P., and Sibuet, M.: First observations of deep-sea coral reefs along the Angola margin, Deep-sea Res. Pt. II, 56, 2394–2403, doi:10.1016/j.dsr2.2009.04.014, 2009.

Liebetrau, V., Eisenhauer, A., and Linke, P.: Cold seep carbonates and associated cold-water corals at the Hikurangi Margin, New Zealand: new insights into fluid pathways, growth structures and geochronology, Mar. Geol., 272, 307–318, doi:10.1016/j.margeo.2010.01.003, 2010.

León, R., Somoza, L., Medialdea, T., Vázquez, J. T., González, F. J., López-González, N., Casas, D., del Pilar Mata, M., del Fernández-Puga, C., Giménez-Moreno, C. J., and Díaz-del-Río, V.: New discoveries of mud volcanoes on the Moroccan Atlantic continental margin (Gulf of Cádiz): morpho-structural characterization, Geo-Mar. Lett., 32, 473–488, doi:10.1007/s00367-012-0275-1, 2012.

Magalhães, V. H., Pinheiro, L. M., Ivanov, M. K., Kozlova, E., Blinova, V., Kolganova, J., Vasconcelos, C., McKenzie, J. A., Bernasconi, S. M., Kopf, A., Díaz-del-Río, V., González, F. J., and Somoza, L.: Formation processes of methane-derived authigenic carbonates from the Gulf of Cádiz, Sediment. Geol., 243–244, 155–168, doi:10.1016/j.sedgeo.2011.10.013, 2012.

Margreth, S., Gennari, G., Rüggeberg, A., Comas, M. C., Pinheiro, L. M., and Spezzferri, S.: Growth and demise of cold-water coral ecosystems on mud volcanoes in the West Alboran Sea: The messages from planktonic and benthic foraminifera, Mar. Geol., 282, 26–39, doi:10.1016/j.margeo.2011.02.006, 2011.

Martin, M.: Cutadapt removes Adapter Sequences from High-Throughput Sequencing Reads, EMBnet.jounal, 10–12, doi: 10.14806/ej.17.1.200, 2011.

McCulloch, M., Falter, J., Trotter, J., and Montagna, P.: Coral resilience to ocean acidification and global warming through pH up-regulation. Nat. Clim. Change, 2(8), 623–627, doi: 10.1038/nclimate1473, 2012.

Medialdea, T., Somoza, L., Pinheiro, L. M., Fernández-Puga, M. C., Vázquez, J. T., León, R., Ivanov, M. K., Magalhães, V., Díaz-del-Río, V., and Vegas, R.: Tectonics and mud volcano development in the Gulf of Cádiz, Mar. Geol., 261, 48–63, doi:10.1016/j.margeo.2008.10.007, 2009.

Mortensen, P. B., Hovland, M. T., Fossa, J. H., and Furevik, D. M.: Distribution, abundance and size of *Lophelia pertusa* coral reefs in mid Norway in relation to seabed characteristics, J. Mar. Biol. Assoc. UK, 81, 581–597, doi:10.1017/S002531540100426X, 2001.

Movilla, J., Gori, A., Calvo, E., Orejas, C., López-Sanz, À., Domínguez-Carrió, C., Grinyó, J., and Pelejero, C.: Resistance of two Mediterranean cold-water coral species to low-pH conditions, Water, 6(1), 59–67, 2014.

Myers, J.L., and Richardson, L.L.: Adaptation of cyanobacteria to the sulfide-rich microenvironment of black band disease of coral, FEMS Microbiol. Ecol., 67, 242–251, doi:10.1111/j.1574-6941.2008.00619.x, 2009.

Nakamura, T., Nadaoka, K., Watanabe, A., Yamamoto, T., Miyajima, T., and Blanco, A. C.: Reef-scale modeling of coral calcification responses to ocean acidification and sea-level rise, Coral Reefs, 37, 2018.

Peckmann, J., Reimer, A., Luth, U., Luth, C., Hansen, B.T., Heinicke, C., Hoefs, J., and Reitner, J.: Methane-derived carbonates and authigenic pyrite from the northwestern Black Sea, Mar. Geol., 177, 129–150, doi:10.1016/S0025-3227(01)00128-1, 2001.

Peckmann, J., and Thiel, V.: Carbon cycling at ancient methane–seeps, Chem. Geol., 205 (3), 443–467, doi:10.1016/j.chemgeo.2003.12.025, 2004.

Petersen, J. M., and Dubilier, N.: Methanotrophic symbioses in marine invertebrates, Env. Microbiol. Rep., 1(5), 319–335, doi:10.1111/j.1758-2229.2009.00081.x, 2009.

Pinheiro, L. M., Ivanov, M. K., Sautkin, A., Akhmanov, G., Magalhães, V. H., Volkonskaya, A., Monteiro, J. H., Somoza, L., Gardner, J., Hamouni, N., and Cunha, M. R.: Mud volcanism in the Gulf of Cádiz: results from the TTR-10 cruise, Mar. Geol., 195, 131–151, doi:10.1016/S0025-3227(02)00685-0, 2003.

Rädecker, N., Pogoreutz, C., Voolstra, C. R., Wiedenmann, J., and Wild, C.: Nitrogen cycling in corals: The key to understanding holobiont functioning?, Trends Microbiol., 23 (8), 490–497, doi:10.1016/j.tim.2015.03.008, 2015.

Reitner, J., Gauret, P., Marin, F., and Neuweiler, F.: Automicrites in a modern marine microbialite. Formation model via organic martices (Lizard Island, Great Barrier Reef, Australia), Bull.-Inst. Oceanogr. Monaco, 14, 237–263, 1995.

Reitner, J., Blumenberg, M., Walliser, E. -O., Schäfer, N., and Duda, J. -P.: Methane-derived carbonate conduits from the late Aptian of Salinac (Marne Bleues, Vocontian Basin, France): Petrology and biosignatures, Mar. Petrol. Geol., 66 (3), 641–652, doi:10.1016/j.marpetgeo.2015.05.029, 2015.

Reitner, J., Peckmann, J., Blumenberg, M., Michaelis, W., Reimer, A., and Thiel, V.: Concretionary methane-seep carbonates and associated microbial communities in Black Sea sediments, Palaeogeogr., Palaeoclimatol., Palaeocl., 227, 18–30, doi:10.1016/j.palaeo.2005.04.033, 2005.

Roberts, J. M., Long, D., Wilson, J. B., Mortensen, P. B., and Gage, J. D.: The cold-water coral *Lophelia pertusa* (Scleractinia) and enigmatic seabed mounds along the north-east Atlantic margin: are they related?, Mar. Pollut. Bull., 46, 7–20, doi:10.1016/S0025-326X(02)00259-X, 2003.

Roberts, J. M., Wheeler, A. J., and Freiwald, A.: Reefs of the deep: the biology and geology of cold-water coral ecosystems, Science, 312 (5773), 543–547, doi:10.1126/science.1119861, 2006.

Roberts, J. M., Wheeler, A., Freiwald, A., and Cairns, S. (Eds.): Cold-water corals: the biology and geology of deep-sea coral habitats, Cambridge University Press, Cambridge, United Kingdom, 2009.

Rodrigues, C. F., Cunha, M. R., Génio, L., and Duperron, S.: A complex picture of associations between two host mussels and symbiotic bacteria in the Northeast Atlantic, Naturwissenschaften, 100, 21–31, doi:10.1007/s00114-012-0985-2, 2013.

Rogers, A. D.: The Biology of *Lophelia pertusa* (Linnaeus 1758) and other Deep-Water Reef-Forming Corals and Impacts from Human Activities, Int. Rev. Hydrobiol., 84 (4), 315–406, doi:10.1002/iroh.199900032, 1999.

Rueda, J. L., González-García, E., Krutzky, C., López-Rodríguez, J., Bruque, G., López-González, N., Palomino, D., Sánchez, R. F., Vázquez, J. T., Fernández-Salas, L. M., and Díaz-del-Río, V.: From chemosynthetic-based communities to cold-water corals: Vulnerable deep-sea habitats of the Gulf of Cádiz, Mar. Biodiver., 46, 473–482, doi:10.1007/s12526-015-0366-0, 2016.

Sánchez-Guillamón, O., García, M. C., Moya-Ruiz, F., Vázquez, J. T., Palomino, D., Fernández-Puga, M. C., and Sierra, A.: A preliminary characterization of greenhouse gas (CH_4 and CO_2) emissions from Gulf of Cádiz mud volcanoes, VIII Symposium MIA15, 2015.

Somoza, L., Ercilla, G., Urgorri, V., León, R., Medialdea, T., Paredes, M., González, F. J., and Nombela, M. A.: Detection and mapping of cold-water coral mounds and living *Lophelia* reefs in the Galicia Bank, Atlantic NW Iberia margin, Mar. Geol., 349, 73–90, doi:10.1016/j.margeo.2013.12.017, 2014.

Somoza, L., León, R., Ivanov, M. Fernández-Puga, M. C., Gardner, J. M., Hernández-Molina, F. J., Pinheiro, L. M., Rodero, J., Lobato, A., Maestro, A., Vázquez, J. T., Medialdea, T., and Fernández-Salas, L. M.: Seabed morphology and hydrocarbon seepage in the Gulf of Cádiz mud volcano area: Acoustic imagery, multibeam and ultra-high resolution seismic data, Mar. Geol., 195, 153–176, doi:10.1016/S0025-3227(02)00686-2, 2003.

Sorokin, Y. I.: Coral reef ecology, Springer, Germany, 1995.

Suess, E, and Whiticar, M. J.: Methane-derived CO_2 in pore fluids expelled from the Oregon subduction zone, Palaeogeogr., Palaeoclimatol., Palaeocl., 71, 119–136, doi:10.1016/0031-0182(89)90033-3, 1989.

Swart, P. K.: Carbon and Oxygen Isotope Fractionation in ScleracUnian Corals: a Review, Earth-Sci. Rev., 19, 51–80, 1983.

Thiel, V., Peckmann, J., Seifert, R.,Wehrung, P., Reitner, J., and Michaelis, W.: Highly isotopically depleted isoprenoids: molecular markers for ancient methane venting, Geochim. Cosmochim. Ac., 63, 3959–3966, doi:10.1016/S0016-7037(99)00177-5, 1999.

Thiel, V., Peckmann, J., Richnow, H.-H., Luth, U., Reitner, J., and Michaelis, W.: Molecular signals for anaerobic methane oxidation in Black Sea seep carbonates and a microbial mat, Mar. Chem. 73, 97–112, doi:10.1016/S0304-4203(00)00099-2, 2001.

Thiem, Ø., Ravagnan, E., Fosså, J. H., and Berntsen, J.: Food supply mechanisms for cold- water corals along a continental shelf edge, J. Marine Syst., 26, 1481–1495, doi:10.1016/j.jmarsys.2005.12.004, 2006.

Vandorpe, T., Martins, I., Vitorino, J., Hebbeln, D., García-García, M., and Van Rooij, D.: Bottom currents and their influence on the sedimentation pattern in the El Arraiche mud volcano province, southern Gulf of Cádiz, Mar. Geol., 378, 114–126, doi:10.1016/j.margeo.2015.11.012, 2016.

Vandorpe, T., Wienberg, C., Hebbeln, D., Van den Berghe, M., Gaide, S., Wintersteller, P., and Van Rooij, D.: Multiple generations of buried cold-water coral mounds since the Early-Middle Pleistocene Transition in the Atlantic Moroccan Coral Province, southern Gulf of Cádiz, Palaeogeogr., Palaeoclimatol., Palaeocl., 485, 293–304, doi:10.1016/j.palaeo.2017.06.021, 2017.

Van Rensbergen, P., Depreiter, D., Pannemans, B., Moerkerke, G., Van Rooij, D., Marsset, B., Akhmanov, G., Blinova, V., Ivanov, M., Rachidi, M., Magalhães, V., Pinheiro, L., Cunha, M., and Henriet, J.P.: The Arraiche mud volcano field at the Moroccan Atlantic slope, Gulf of Cádiz, Mar. Geol., 219, 1–17, doi:10.1016/j.margeo.2005.04.007, 2005.

Van Rooij, D., Blamart, D., De Mol, L., Mienis, F., Pirlet, H., Whermann, L. M., …, Henriet, J. -P.: Cold-water coral mounds on the Pen Duick Escarpment, Gulf of Cádiz: The MiCROSYSTEMS project approach, Mar. Geol., 282, 102–117, doi:10.1016/j.margeo.2010.08.012, 2011.

Watling, L., France, S. C., Pante, E., and Simpson, A.: Biology of Deep-Water Octocorals, in: Advances in Marine Biology Volume 60, Lesser, M. (Eds.), Academic Press, London, United Kingdom, 41–122, 2011.

Webster, N. S., Negri, A. P., Botté, E. S., Laffy, P. W., Flores, F., Noonan, S., Schmidt, C., and Uthicke, S.: Host-associated coral reef microbes respond to the cumulative pressures of ocean warming and ocean acidification Sci. Rep.-UK, 6, doi:10.1038/srep19324, 2016.

Wheeler, A. J., Beyer, A., Freiwald, A., de Haas, H., Huvenne, V. A., Kozachenko, M., Olu-Le Roy, K., and Opderbecke, J.: Morphology and environment of cold-water coral carbonate mounds on the NW European margin, Int. J. Earth Sci., 96, 37–56, doi:10.1007/s00531-006-0130-6, 2007.

Wehrmann, L. M. Templer, S. P., Brunner, B., Bernasconi, S. M., Maignien, L., and Ferdelman, T. G.: The imprint of methane seepage on the geochemical record an early diagenetic processes in cold-water coral mounds on Pen Duick Escarpment, Gulf of Cádiz, Mar. Geol., 118–137, doi:10.1016/j.margeo.2010.08.005, 2011.

Wienberg, C., Hebbeln, D., Fink, H. G., Mienis, F., Dorschel, B., Vertino, A., López-Correa, M., and Freiwald, A.: Scleractinian cold-water corals in the Gulf of Cádiz—first clues about their spatial and temporal distribution, Deep-sea Res. Pt. I, 56 (10), 1873–1893, doi:10.1016/j.dsr.2009.05.016, 2009.

Wienberg, C., and Titschack, J.: Framework-forming scleractinian cold-water corals through space and time: a late Quaternary North Atlantic perspective, in: Marine Animal Forests: The Ecology of Benthic Biodiversity Hotspots, Rossi, S., Bramanti, L., Gori, A., and Orejas, C. (Eds.), Springer, Cham, Switzerland, 1–34, 2015.

Yilmaz, P., Parfrey, L.W., Yarza, P., Gerken, J., Pruese, E., Quast, C., Schweer, T., Peplies, J., Ludwig, W., and Glöckner, F. O.: The SILVA and 'All-species Living Tree Project (LTP)' taxonomic frameworks, Nucleic Acids Res., 42, D643–D648, doi:10.1093/nar/gkt1209, 2014.

Zhang, J., Kobert, K., Flouri, T., and Stamatakis, A.: PEAR: a fast and accurate Illumina Paired-End reAd merger, Bioinformatics, 30 (5), 614–620, doi:10.1093/bioinformatics/btt593, 2014.

Zoccola, D. Ganot, P., Bertucci, A., Caminit-Segonds, N., Techer, N., Voolstra, C. R., Aranda, M., Tambutté, E., Allemand, D., Casey, J. R., and Tambutté, S.: Bicarbonate transporters in corals point towards a key step in the evolution of cnidarian calcification, Sci. rep.-UK, 5, 2015.

Table 1. General description and characterization of recovered samples for this study in the Al Gacel MV and Northern Pompeia Coral Ridge. Please note that samples D10-R3 and D11-R8 were carbonates with embedded corals (see **Fig. 7** for more details).

	Site description	Coordinates	Depth (m)	Type	Sample
Al Gacel MV	Base of volcano characterized by non-chemosynthetic fauna	35° 26.51' N -6° 58.22' W	850 – 890	Carbonate	D10-R3
	Active pockmark	35° 26.47' N -6° 58.27' W	790	Carbonate	D10-R7
				Water	D10-N4
					D10-C5
					D10-C8
	Summit with metric carbonate blocks	35° 26.48' N -6° 58.35' W	763	Carbonate	D11-R8
		35° 26.48' N -6° 58.37' W	760	Water	D11-N9
					D11-C10
Northern Pompeia Coral Ridge	Sulfide-oxidizing bacterial mats and shells of chemosynthetic bivalves	35° 26.77' N -6° 59.94' W	829	Necrotic fragment of a living *Madrepora oculata* coral	D03-B1

Table 2. *In-situ* water variables measured during sampling with ROV sensors.

	D10-R3	D10-R7	D11-R8	D03-B1
Temperature (°C)	10.07	10.5	10.02	10.04 – 10.05
Conductivity (mS/cm)	39.13 – 39.62	39.05 – 39.43	-	-
Salinity (ppt)	-	-	35.56 – 35.86	35.67 – 35.91
Saturation of dissolved oxygen (%)	53.64 – 54.69	54.02 – 54.35	51.95 – 53.92	52.46 – 56.22
Dissolved oxygen (mg/l)	4.81 – 4.90	4.85 – 4.88	4.66 – 4.84	4.71 – 5.09
Density (kg/m^3)	31.03 – 31.42	30.94 – 31.24	30.92 – 31.08	31.26 – 31.41

Table 3. On site measurements of soluble Fe^{2+} and S^{2+} values from seawater and pore-water. Please note that samples D10-C5, D10-C8 and D10-N4 were taken from the same site as the authigenic carbonate D10-R7 (see **Fig. 2**). d.l. = detection limit.

Sample	Type	Fe^{2+} (µM)	S^{2+} (µM)	pH	ORP (mV)
D10-C5 (0 – 6 cm)	Pore-water	0.94	< d.l.	-	-
D10-C5 (6 –16 cm)		1.27	< d.l.	-	-
D10-C8 (0 – 6 cm)		2.70	< d.l.	-	-
D10-C8 (6 –16 cm)		1.74	0.23	-	-
D10-N4	Sea-water	0.57	< d.l.	7.88	136
D11-C10 (0 – 5 cm)	Pore-water	2.39	< d.l.	-	-
D11-C10 (5 – 15 cm)		5.32	0.47	-	-
D11-N9	Seawater	0.31	< d.l.	7.85	257

764 **Table 4.** Stable carbon and oxygen isotopes ($\delta^{13}C$, $\delta^{18}O$) of samples from the Al Gacel MV and the Northern
765 Pompeia Coral Ridge.

Location	Sample	Origin of the carbonate	Identification number in Fig. 7	$\delta^{18}O$ (‰)	$\delta^{13}C$ (‰)
Al Gacel MV	D10-R3	Coral skeleton	1	2.35	−5.58
		Authigenic carbonate	2	3.37	−20.07
			3	3.60	−26.68
			4	3.70	−20.79
			5	3.45	−22.43
			6	3.80	−20.70
		Coral skeleton	7	3.28	−2.23
		Authigenic carbonate	8	3.83	−25.16
			9	3.63	−25.29
			10	3.91	−18.38
			11	3.60	−24.18
			12	3.55	−25.34
			13	3.56	−25.15
		Coral skeleton	14	3.50	−2.09
		Authigenic carbonate	15	3.92	−21.89
	D10-R7	Authigenic carbonate	21	2.90	−26.36
			22	3.15	−28.77
			23	2.94	−22.91
			24	2.67	−21.13
			25	2.37	−24.70
			26	2.56	−23.60
	D11-R8	Coral skeleton	16	1.49	−4.91
			17	2.13	−2.99
			18	1.74	−4.22
		Authigenic carbonate	19	5.60	−14.82
			20	5.55	−14.74
Northern Pompeia Coral Ridge	D03-B1	Coral skeleton	1.1	−0.38	−7.93
			1.2	−0.86	−7.77
			1.3	−0.51	−7.35
			1.5	1.15	−5.26
			1.4	−1.03	−8.08
			1.6	0.69	−5.96
			1.7	0.54	−6.42

766

Table 4. Continued

Location	Sample	Origin of the carbonate	Identification number in Fig. 7	$\delta^{18}O$ (‰)	$\delta^{13}C$ (‰)
Northern Pompeia Coral Ridge	D03-B1	Coral skeleton	3.1	1.59	−2.08
			3.2	−0.31	−6.27
			3.3	−0.89	−6.78
			3.4	−0.94	−6.73
			3.5	1.84	−2.21
			3.6	2.26	−1.39
			3.7	1.74	−2.87

Table 5. Stable carbon isotopic composition ($\delta^{13}C$) of selected lipid biomarkers (in **Figure 10**). (*) Please note that crocetane in D11-R8 coelutes with phytane. n.d. = not detected.

Compound	D10-R7 (‰)	D11-R8 (‰)
n-C_{17}	n.d.	–33.0
n-C_{18}	n.d.	–31.8
n-C_{19}	n.d.	–31.1
n-C_{20}	n.d.	–30.8
n-C_{21}	n.d.	–31.5
n-C_{22}	n.d.	–31.7
Crocetane*	–101.2	–57.2
PMI	–102.9	–74.3

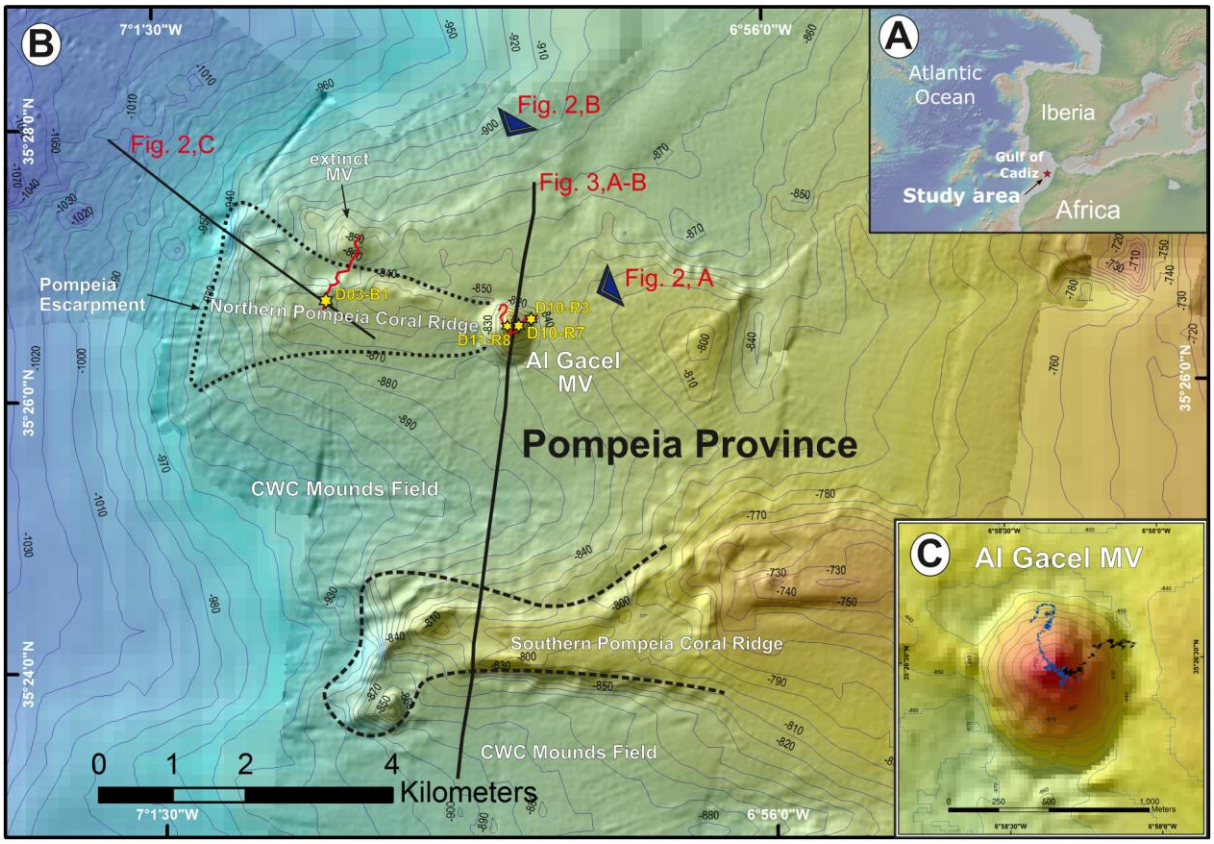

780

781 **Figure 1**. Bathymetric map of the study area. **A**: location of the Gulf of Cádiz between Spain, Portugal and
782 Morocco. The study area is marked with a red star; **B**: the Pompeia Province including its different morphological
783 features. Red lines indicate ROV-paths, yellow stars mark sampling sites; **C**: detailed map of the Al Gacel MV
784 including pathways of Dive 10 and 11 (black and blue lines, respectively). Further details of the area are provided
785 in **Figs. 2** and **3**.

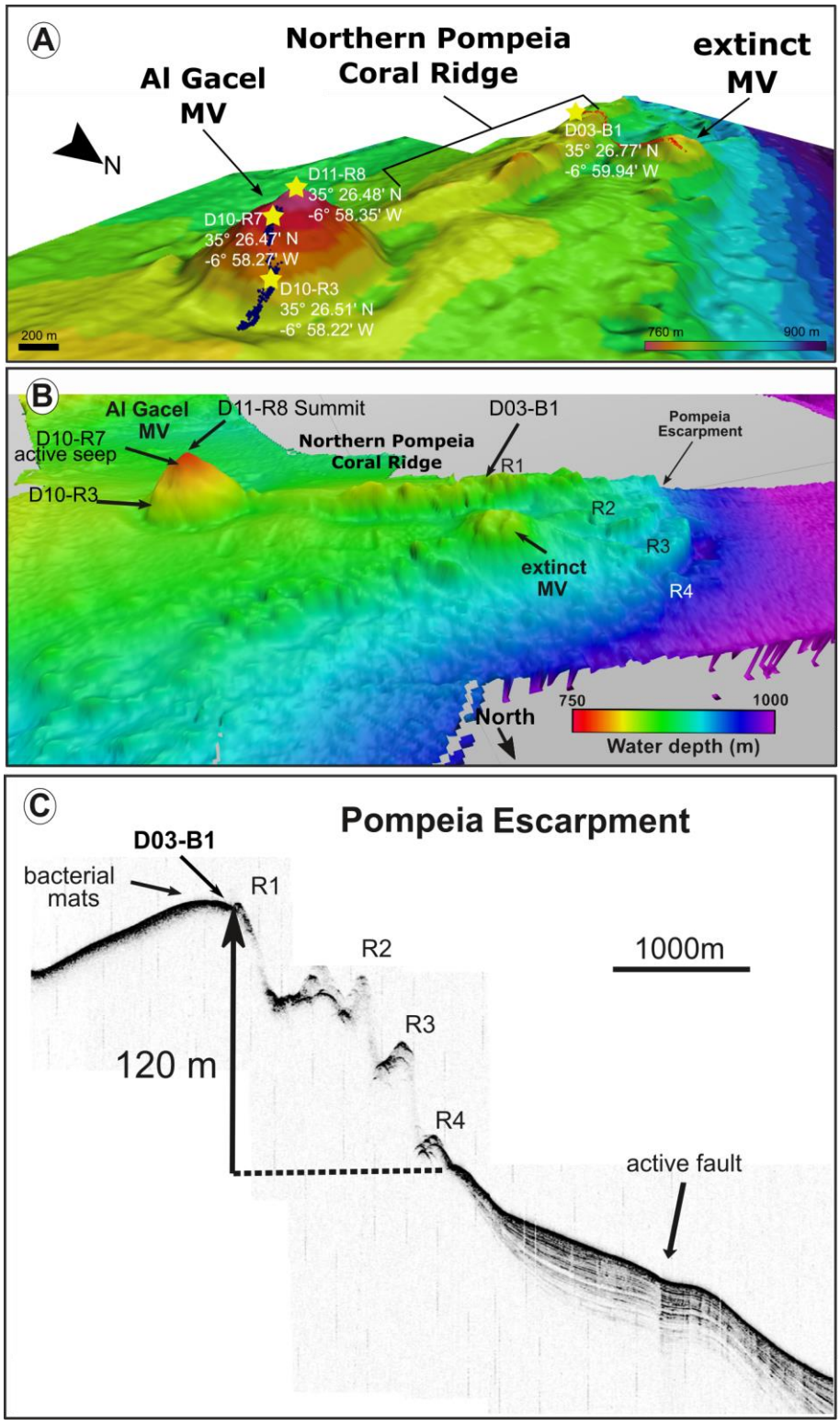

Figure 2. Bathymetric and seismic maps showing morphological features in northern Pompeia Province. **A–B**: bathymetric maps showing the Al Gacel MV, the Northern Pompeia Coral Ridge and the extinct MV. Yellow stars mark sampling sites. **C**: ultra-high seismic profile of the Pompeia Escarpment, westwards of the Northern Pompeia Coral Ridge.

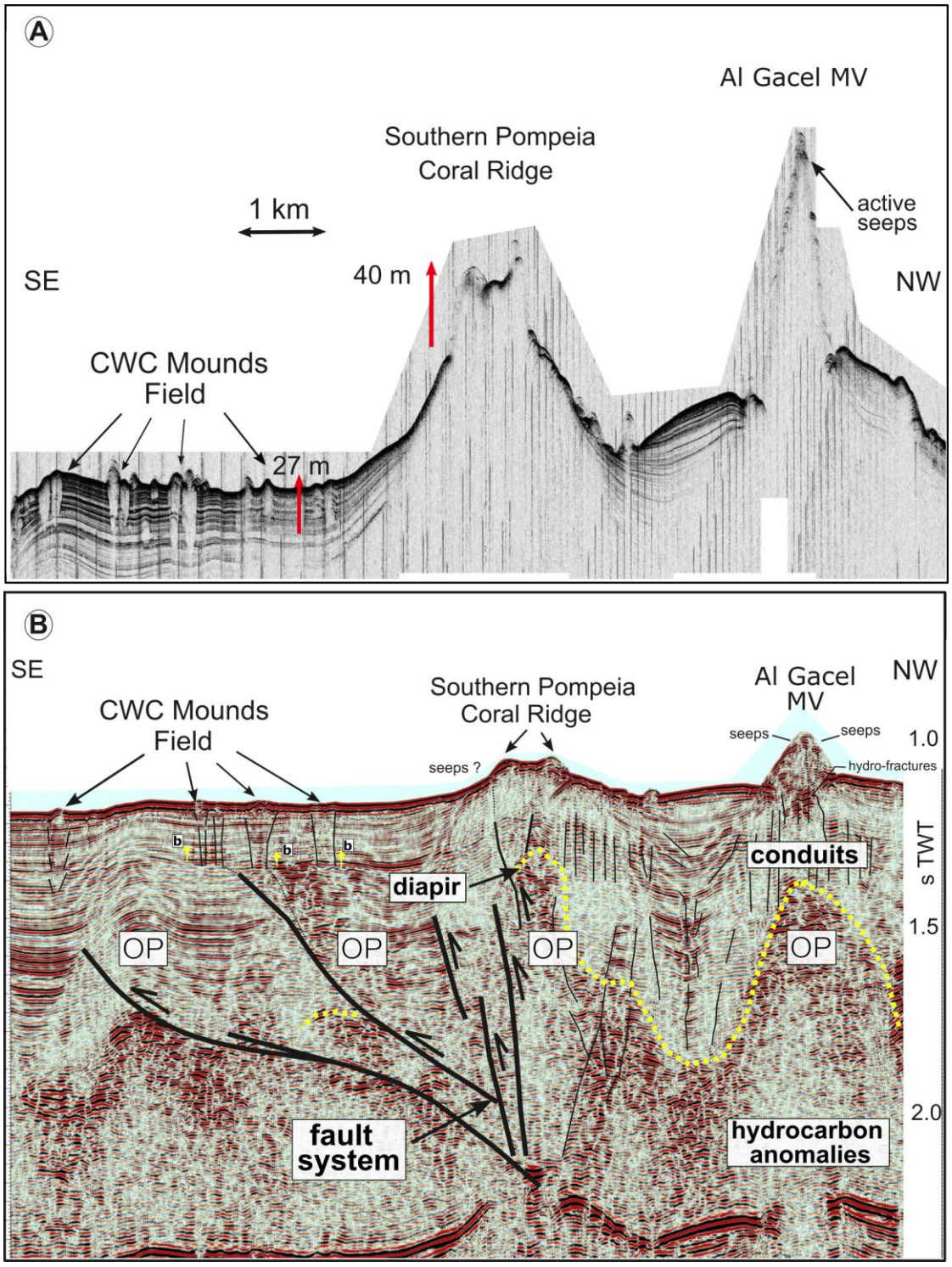

Figure 3. Ultra-high resolution (**A**) and multichannel (**B**) seismic profiles showing geological features in southern Pompeia Province. Note mud diapirism has been described in this area (Vandorpe et al., 2017). OP = overpressure zone.

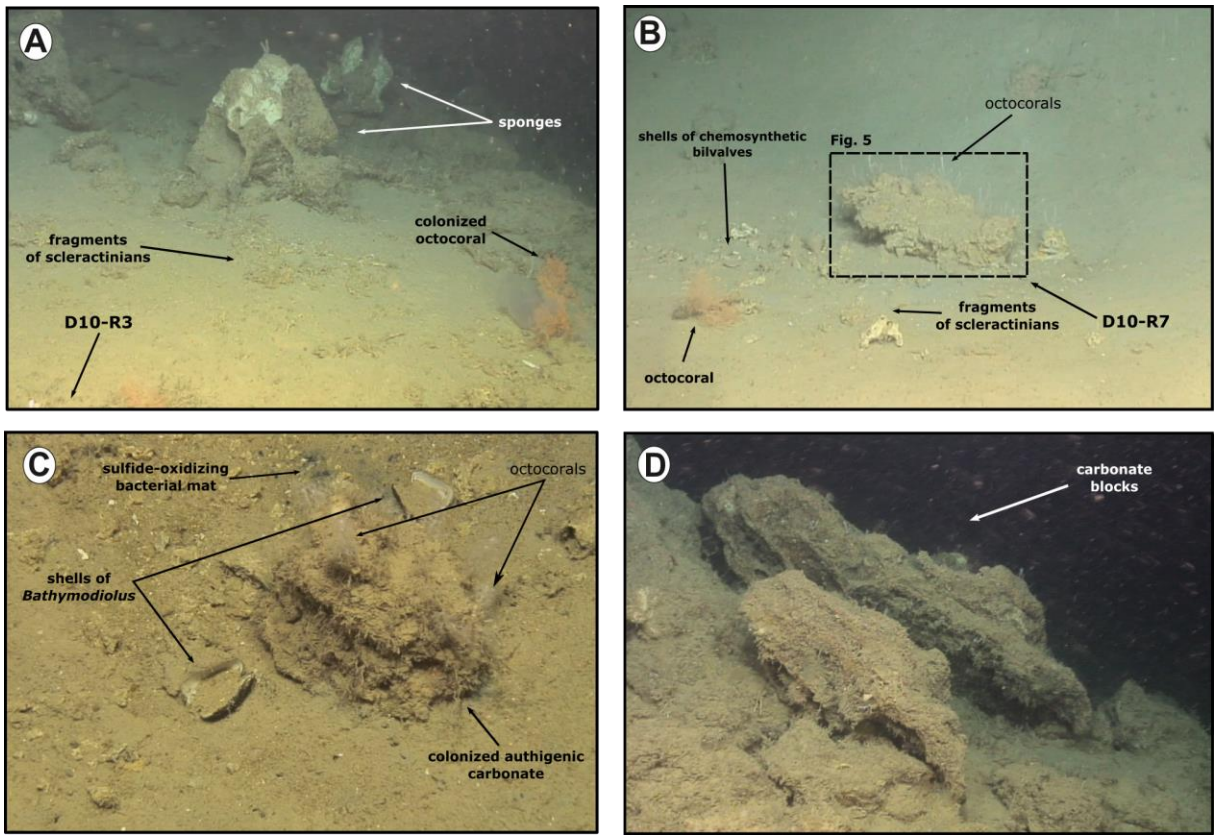

Figure 4. ROV still frames from the Al Gacel MV (Dives 10 and 11). **A**: eastern side of the volcano, displaying a field of sponges, corals and carbonates; **B–C**: active pockmark sites on the east side of the volcano, displaying authigenic carbonate surrounded by shells of chemosynthetic bivalves, fragments of scleractinian and octocorals, as well as sulfide-oxidizing bacterial mats; **D**: metric-sized carbonate blocks located in a slope at the summit of the volcano.

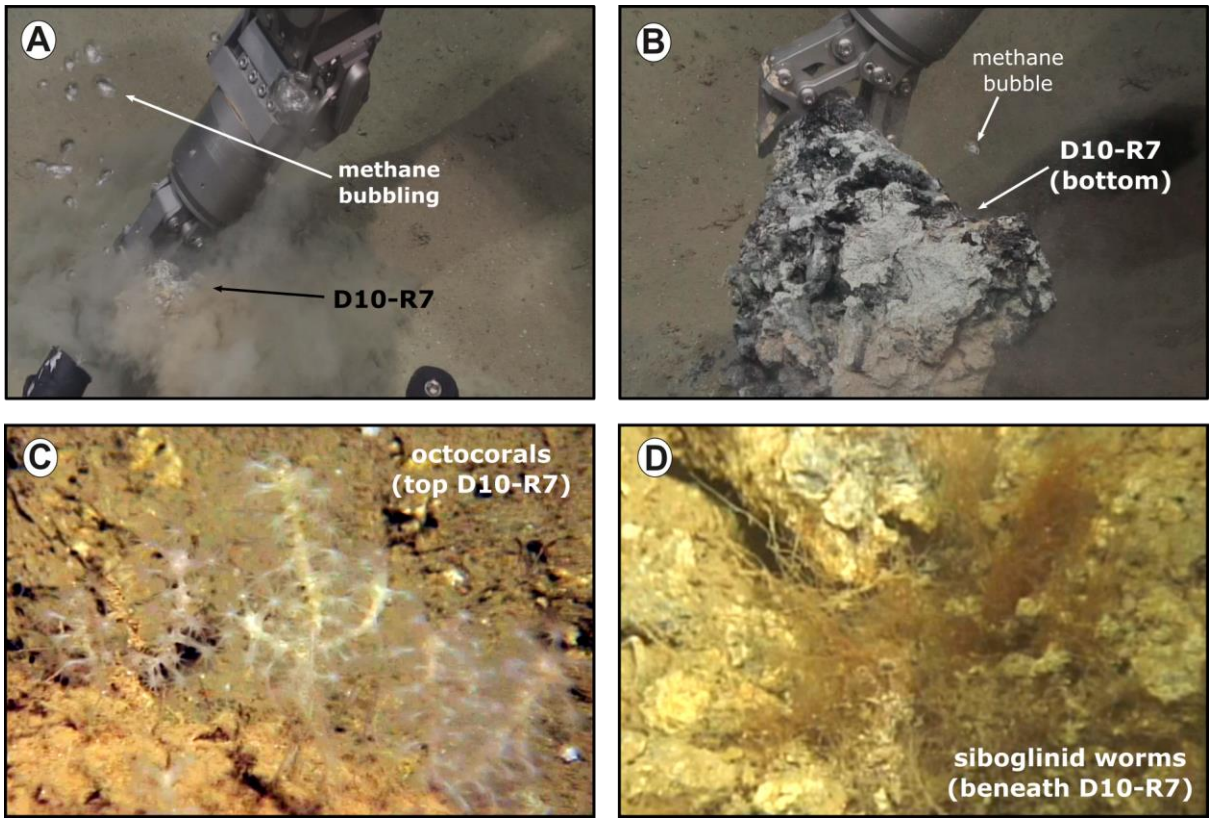

Figure 5. ROV still frames from the active pockmark site shown in **Fig. 4**, **B**. **A–B**: release of bubbles while sampling; **C**: detailed photograph of the octocorals on top of the carbonate; **D**: detailed still frame from siboglinid worms beneath the carbonate.

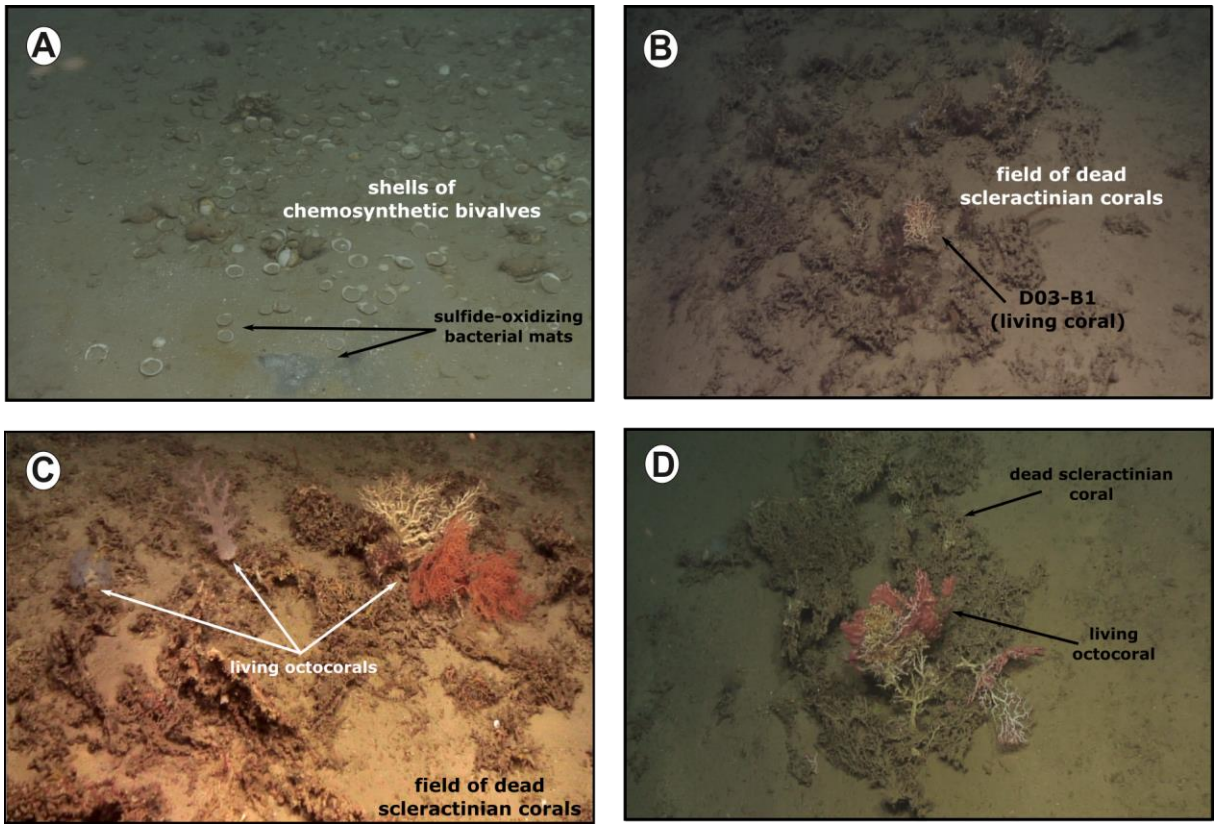

811

812 **Figure 6.** ROV still frames from the Northern Pompeia Coral Ridge and extinct MV (Dive 03), where there is
813 currently a diffused seepage of fluids. **A**: abundant shells of chemosynthetic bivalves with sulfide-oxidizing
814 bacterial mats at the western site of the Northern Pompeia Coral Ridge; **B–D**: field of dead scleractinian-corals
815 colonized by living corals; **D**: still frame from the extinct MV.

816

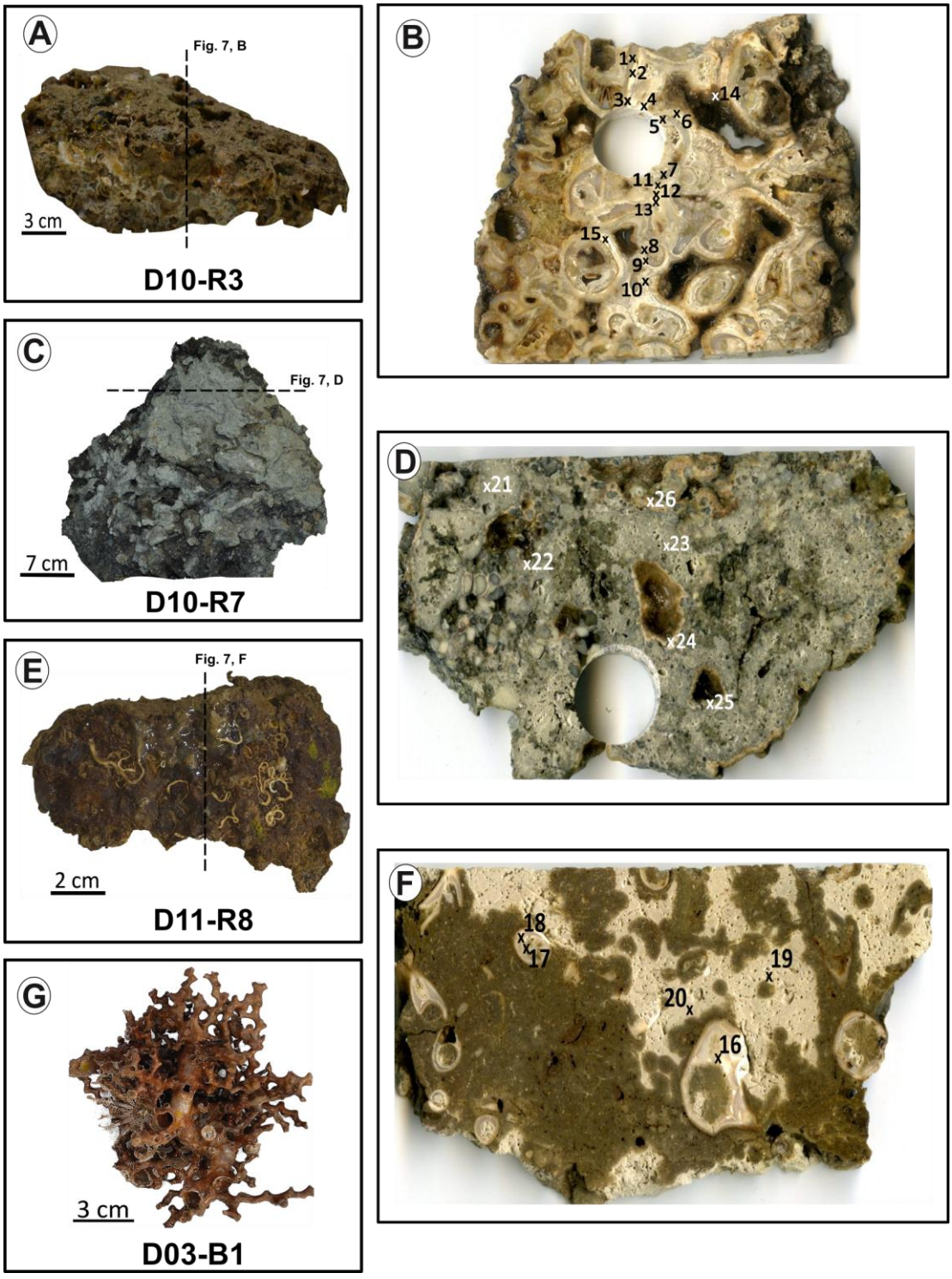

Figure 7. Photographs of analyzed samples including sampling sites for stable carbon and oxygen isotope ($\delta^{13}C$, $\delta^{18}O$) analysis (crosses with numbers). Values of the stable isotopic analyses are found in **Table 2**. **A–B**: D10-R3 carbonate with embedded corals; **C–D**: D10-R7 carbonate with strong H_2S odor; **E–F**: D11-R8 carbonate with embedded corals; **G**: D03-B1 scleractinian-coral fragment, *Madrepora oculata*. Please note that we cannot determine whether the corals were alive or dead the time they were buried by the carbonate.

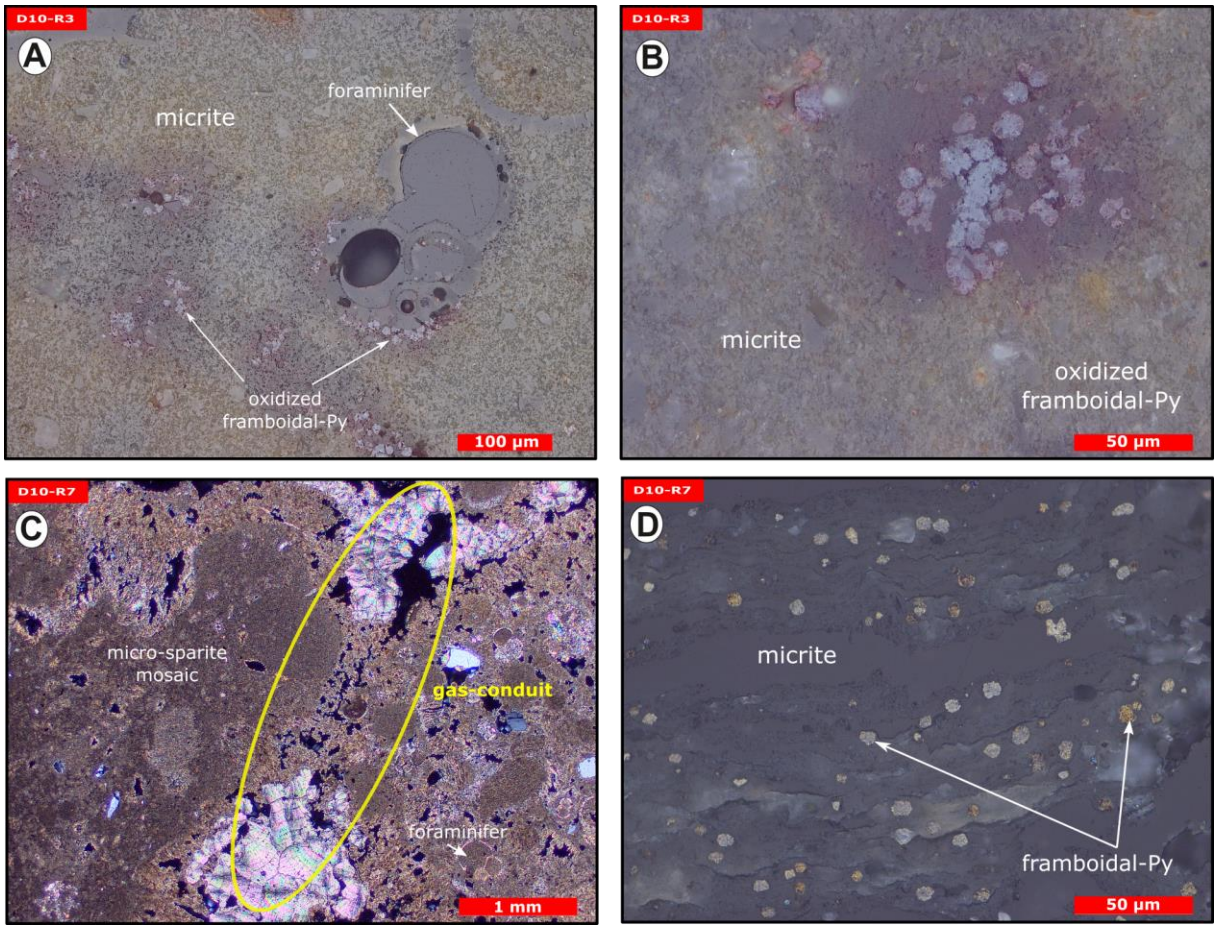

Figure 8. Thin section photographs of MDACs. **A–B**: D10-R3 consisting of a micritic matrix with scattered foraminifers and oxidized framboidal pyrites (reflected light); **C–D**: D10-R7 consisting of micritic and micro-sparitic carbonate with abundant unaltered framboidal pyrites (C, transmitted light; D, reflected light). Please note open voids which represent potential pathways for fluid seepage (yellow circle in C).

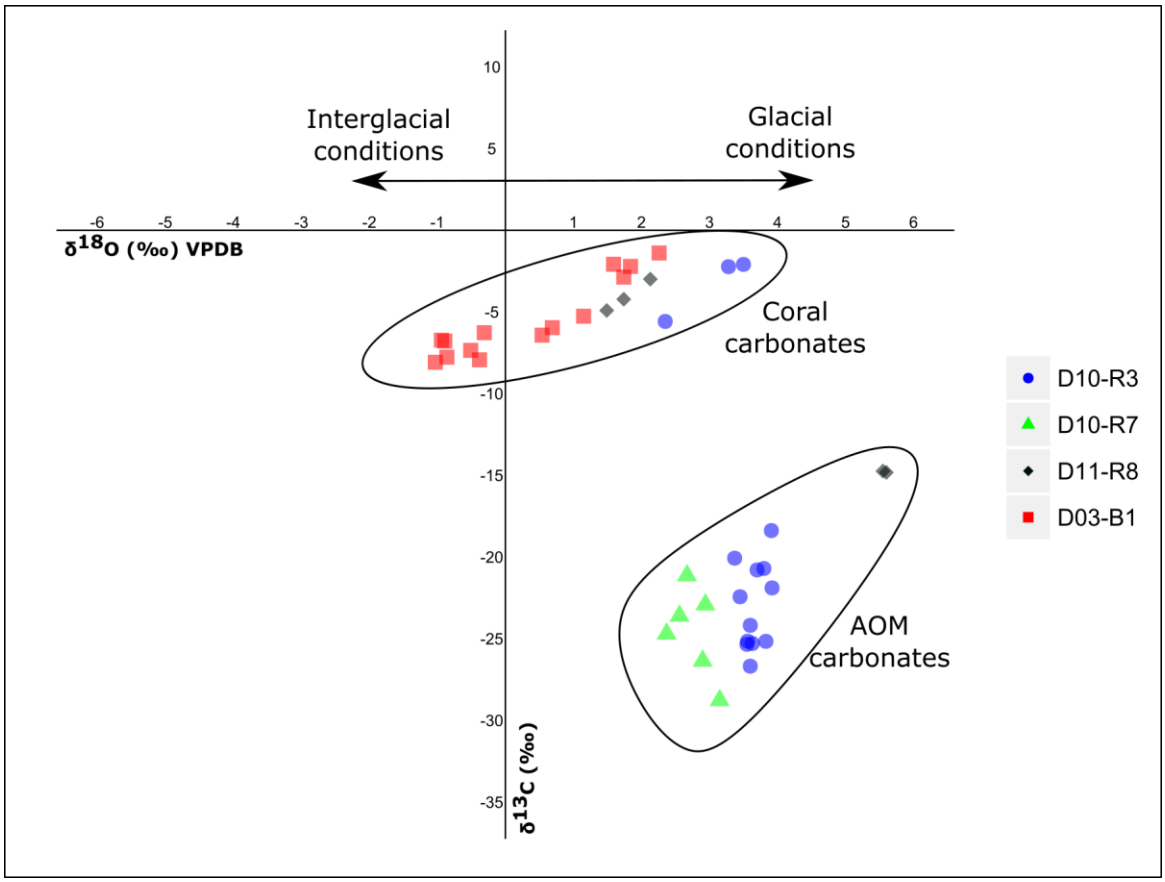

Figure 9. Stable carbon and oxygen isotopes ($\delta^{13}C$, $\delta^{18}O$) of samples from the Al Gacel MV and the Northern Pompeia Coral Ridge (see **Table 3** and **Fig. 7** for precise sampling points).

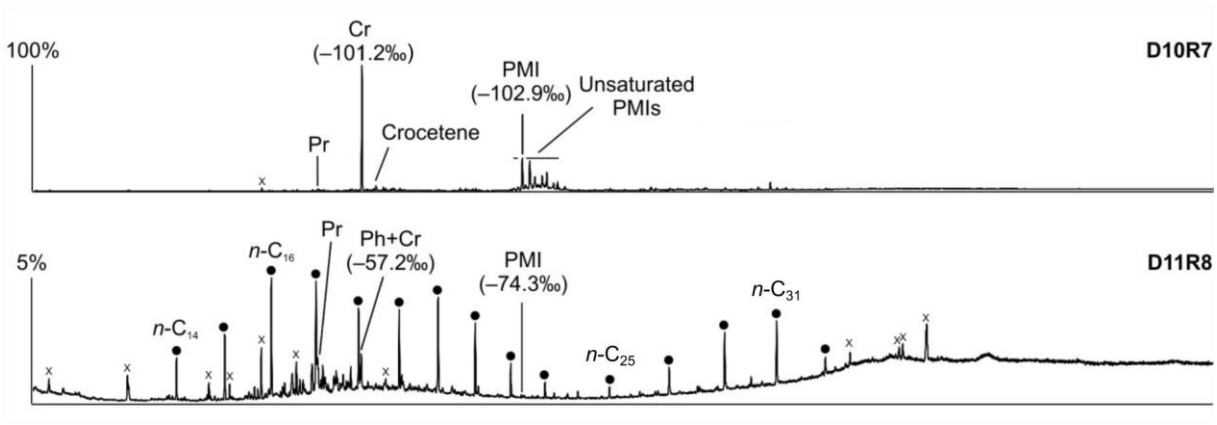

Figure 10. Total ion current (TIC) chromatograms of the analyzed samples. Isotopically depleted acyclic irregular isoprenoids such as Cr and PMI are typically found in settings influenced by the anaerobic oxidation of methane (AOM). Pr = pristane; Ph = phytane; Cr = crocetane; PMI = 2,6,10,15,19-pentamethylicosane; dots = n-alkanes; crosses = siloxanes (septum or column bleeding). Percentage values given on the vertical axes of chromatograms relate peak intensities to highest peak (Cr in D10-R7).

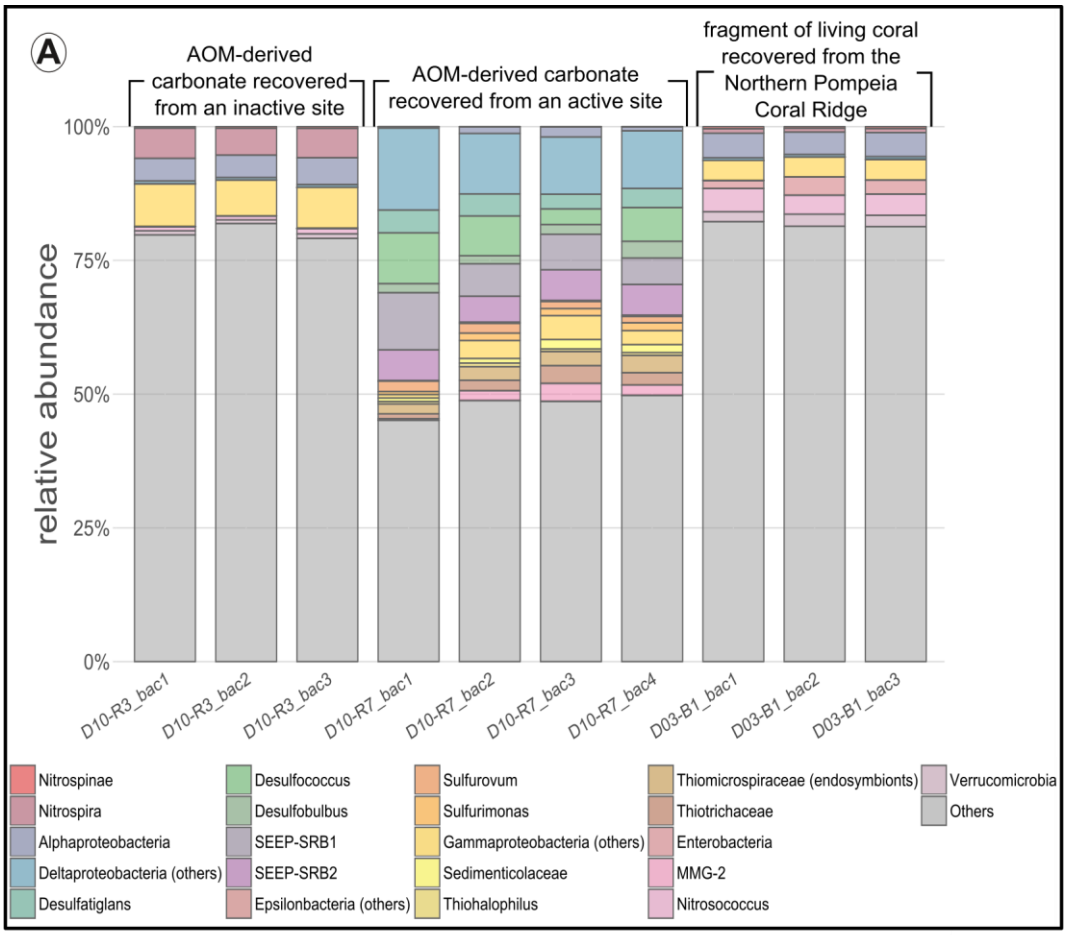
A
AOM-derived carbonate recovered from an inactive site
AOM-derived carbonate recovered from an active site
fragment of living coral recovered from the Northern Pompeia Coral Ridge
relative abundance
100%
75%
50%
25%
0%
D10-R3_bac1
D10-R3_bac2
D10-R3_bac3
D10-R7_bac1
D10-R7_bac2
D10-R7_bac3
D10-R7_bac4
D03-B1_bac1
D03-B1_bac2
D03-B1_bac3
Nitrospinae
Nitrospira
Alphaproteobacteria
Deltaproteobacteria (others)
Desulfatiglans
Desulfococcus
Desulfobulbus
SEEP-SRB1
SEEP-SRB2
Epsilonbacteria (others)
Sulfurovum
Sulfurimonas
Gammaproteobacteria (others)
Sedimenticolaceae
Thiohalophilus
Thiomicrospiraceae (endosymbionts)
Thiotrichaceae
Enterobacteria
MMG-2
Nitrosococcus
Verrucomicrobia
Others

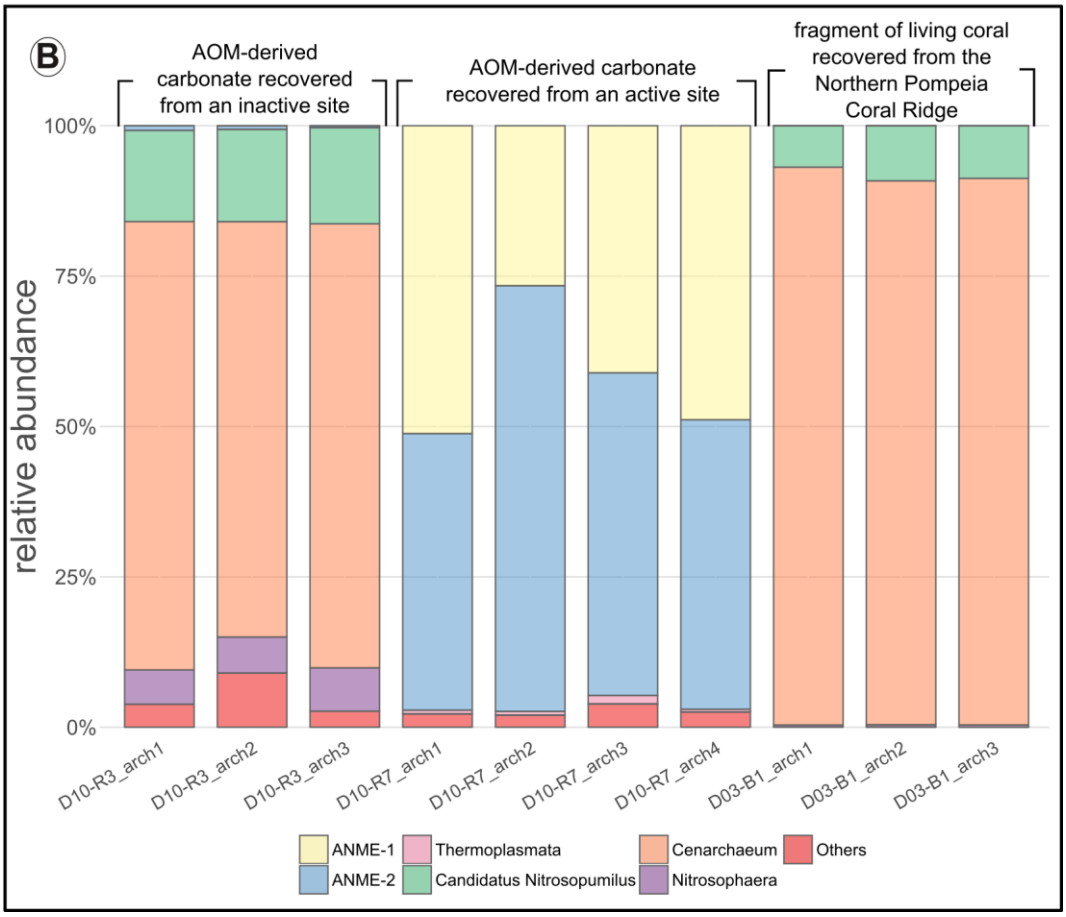
B
AOM-derived carbonate recovered from an inactive site
AOM-derived carbonate recovered from an active site
fragment of living coral recovered from the Northern Pompeia Coral Ridge
relative abundance
100%
75%
50%
25%
0%
D10-R3_arch1
D10-R3_arch2
D10-R3_arch3
D10-R7_arch1
D10-R7_arch2
D10-R7_arch3
D10-R7_arch4
D03-B1_arch1
D03-B1_arch2
D03-B1_arch3
ANME-1
ANME-2
Thermoplasmata
Candidatus Nitrosopumilus
Cenarchaeum
Nitrosophaera
Others

846

847 **Figure 11**. Bar chart representing relative abundances of prokaryotic taxa detected in each sample. **A**: bacterial
848 taxa; **B**: archaeal taxa. In "others" aggrupation is included taxa related to ubiquitous organism normally found in
849 sea- and seepage-related environments, and unclassified organisms. Number of reads per taxa detailed in **Table**
850 **S1** (bacteria) and **Table S2** (archaea).

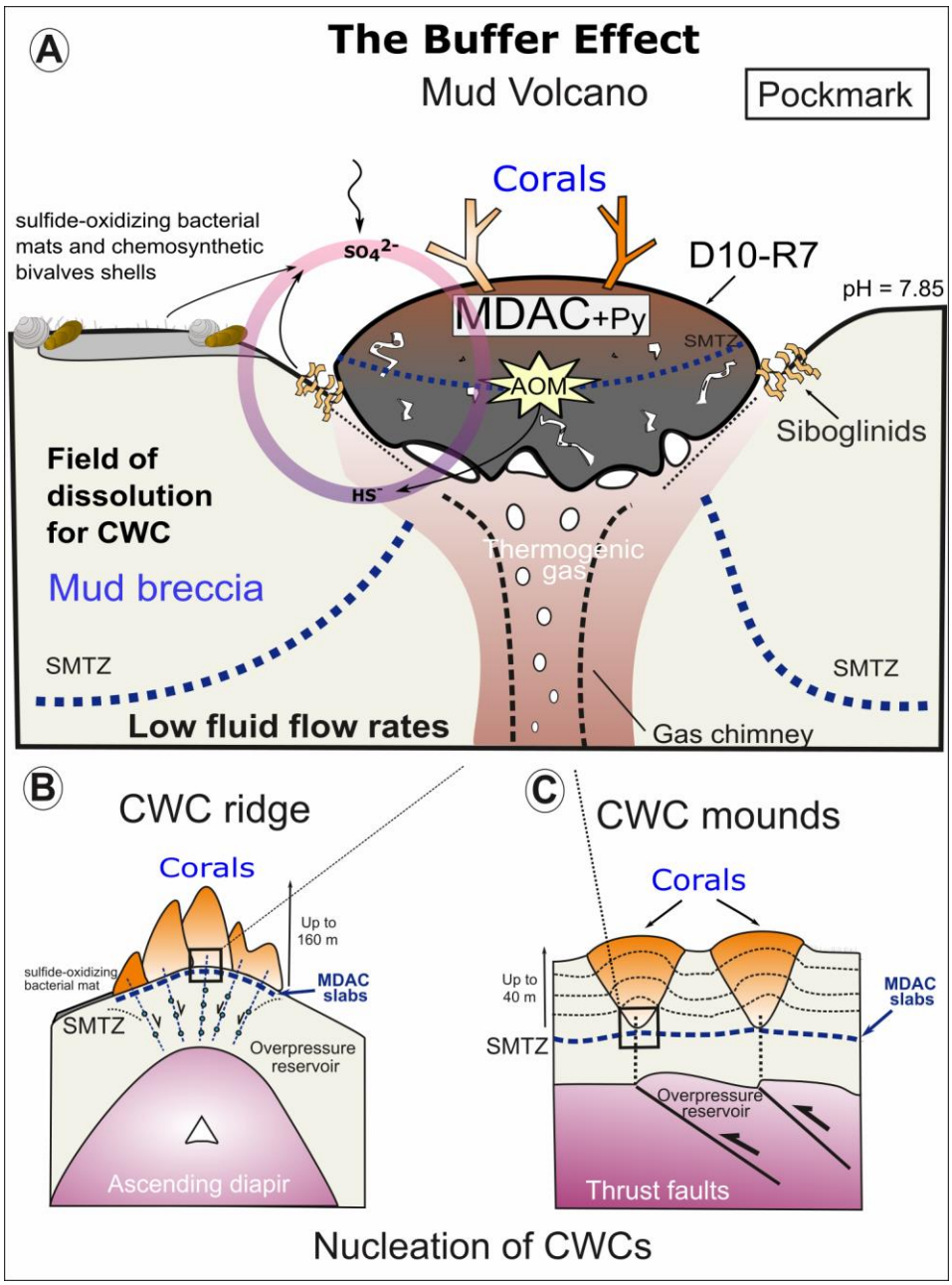

Figure 12. The buffer effect model. **A**: Buffer effect at pockmark sites (e.g. sampling site of D10-R7) where carbonates are formed directly on the bubbling site acting as a cap; **B**: Buffer effect at diapiric ridges where MDAC slabs are formed on the base of the ridge; **C**: Buffer effect at coral mounds where MDAC slabs are formed in deeper layers of the sediment. Py = pyrite, SMTZ: sulfur-methane transition zone.